

arXiv:0908.3450v2 [hep-ph] 15 Sep 2009

Summing loops in QCD: Exclusive Higgs production and the survival probability

J. Miller*

*CENTRA, Departamento de Física, Instituto Superior Técnico (IST),
Av. Rovisco Pais,
1049-001 Lisboa,
Portugal*

ABSTRACT: The Pomeron loop amplitude and the amplitude for the diagram with any general number of loops is derived in the QCD dipole approach. It was found that the major contribution to the amplitude of an arbitrary Pomeron enhanced diagram, is equivalent to the amplitude of the diagram with non interacting Pomerons. This provides the necessary tools for solving the long standing theoretical problem of summing over Pomeron loop diagrams. In this theoretical framework the contribution of the full set of enhanced diagrams to the survival probability is estimated. This enables an accurate prediction for the exclusive cross section for diffractive Higgs production, which includes the suppression factor needed to screen out the full set of hard re-scattering corrections, in QCD.

KEYWORDS: BFKL Pomeron, Triple Pomeron vertex, Higgs boson, summing Pomeron loops, QCD.

*Email: jeremymi@post.tau.ac.il; miller@physics.org

Contents

1. Introduction	1
2. The Pomeron propagator	5
3. The simple Pomeron loop	11
4. The main idea	20
5. Multiple-loop Pomeron enhanced diagrams	23
6. The summation over Pomeron loop diagrams	30
7. The survival probability for exclusive Higgs production	35
8. Conclusion	36
9. Acknowledgements	39
A. The triple Pomeron vertex	39
B. The fan diagram	43

1. Introduction

The main goal of this paper is to solve the unsolved problem of the summation over Pomeron loops, in QCD. In proton proton collisions the main t-channel exchange is the BFKL Pomeron, which is a double t channel gluon exchange with “ladder” gluons in between, as shown in Fig. 1. The BFKL Pomeron can split into two daughter Pomerons and re-merge through the triple Pomeron vertex shown in Fig. 2, forming Pomeron loops. Due to the large size of the triple Pomeron vertex (see for example refs. [1, 2]) Pomeron loop diagrams give a significant contribution to the high energy scattering amplitude in proton proton collisions, which is comparable to the amplitude of the basic diagram of Fig. 1. As such, the scattering amplitude of hadronic reactions requires an accurate estimate for the summation over Pomeron loop diagrams

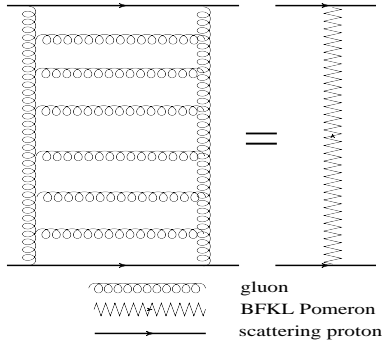


Figure 1: The BFKL Pomeron structure.

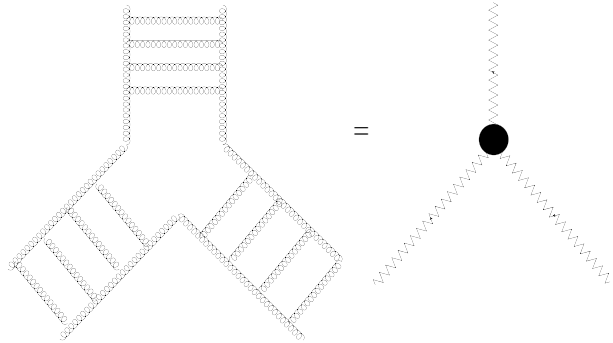


Figure 2: The triple Pomeron vertex.

to be taken into account (for an example of such diagrams, see Fig. 9, Fig. 14 and Fig. 15). Hence the correct algorithm for the summation over Pomeron loops is a result which is in high demand, not just from a theoretical perspective, but also from an experimental point of view. The main practical application of this result is in exclusive diffractive Higgs production, at the LHC.

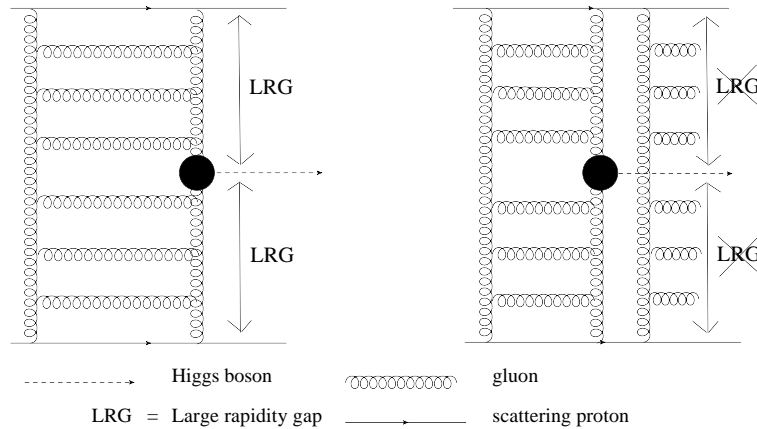


Figure 3: Diffractive production of the Higgs boson through double t-channel gluon exchange. On the left is exclusive Higgs production with large rapidity gaps (LRG) between the Higgs and the emerging protons. On the right is the production of Higgs with extra production which spoils the LRGs, arising from additional inelastic scattering.

The keenly awaited result of the discovery of the Higgs boson at the LHC, is expected to emerge from smashing together two protons, in so-called diffractive Higgs production. Unfortunately, proton-proton scattering results in the production of many other unwanted particles. This makes the process of detecting the Higgs very problematic. The desired result is the production of the Higgs with two large rapidity gaps (LRG) between the Higgs and the emerging protons as shown in the left hand diagram of Fig. 3, which ensures that there is no additional production. The survival of these two large rapidity gaps is quantified by the survival probability. The difficulty in isolating the Higgs signal is characterized by the small value

of the survival probability, which has so far been estimated to be small, and could be even less than 1 % (see detailed estimates in refs. [3, 4]).

Due to the size of the strong coupling, the dominant mechanism for diffractive Higgs production is through the exchange of a t channel gluon between the scattering protons. To ensure that there is no further production, a second t - channel gluon exchanged between the scattering protons is needed to cancel the color flow, as shown in Fig. 3. This colorless double gluon exchange cancels the possibility of the production of additional particles.

The double gluon exchange evolves to the “ladder” structure, as gluons are exchanged between the two t channel gluons, forming the rungs of the ladder (see Fig. 3). This structure is the so called BFKL Pomeron. The energy levels of the BFKL Pomeron are labeled by the BFKL eigenfunction $\omega(n, \nu)$, where n is an integer and ν is a conformal variable which one integrates over, when calculating Feynman diagrams.

Unfortunately, extra parton showers between the scattering protons is inevitable, leading to the production of additional particles that fill up the large rapidity gaps (see Fig. 3 right). Hard re-scattering corrections, namely Pomeron branching which forms loop diagrams and fan diagrams of the type shown in Fig. 4 also contribute to the problem of additional unwanted production. Pomeron loop diagrams and fan diagrams of this kind are called “enhanced” diagrams. The suppression factor needed, to remove the effect of enhanced diagrams on the Higgs cross section, is the “enhanced survival probability” $\langle |S_{\text{enh}}^2| \rangle$.

Pomeron loop diagrams are extremely useful because they include the contribution of “fan diagrams”, Pomeron loops and the contribution of non interacting Pomerons as shown in Fig. 4. As such, summing over the complete set of Pomeron loop diagrams will provide the suppression factor needed for screening out all unwanted particle production, which stems from Pomeron enhanced diagrams. In other words, the summation of Pomeron loops provides the full set of hard re-scattering corrections to the enhanced survival probability $\langle |S_{\text{enh}}^2| \rangle$.

In ref. [3] the one loop Pomeron diagram was calculated in QCD. The result was used to fix the parameters of the mean field approximation (MFA) of Mueller, Patel, Salam and Iancu (MPSI) (see ref. [5]), and using this the summation over Pomeron loops was estimated using the toy model of Kovchegov [6]. In this way the survival probability was found to be potentially as low as 0.4%. This implied that Pomeron loop diagrams give a significant contribution to the survival probability. In ref. [7] we derived a useful expression for the triple Pomeron vertex in the momentum representation, which is the crucial ingredient for calculating any diagram with Pomeron branching and Pomeron loops. Using this we showed that a diagram with an arbitrary number of Pomeron loops reduces to the diagram of non interacting Pomerons. This important step forward, outlined the first method for the summation over Pomeron loop diagrams completely in the QCD approach, and not in the mean field approximation.

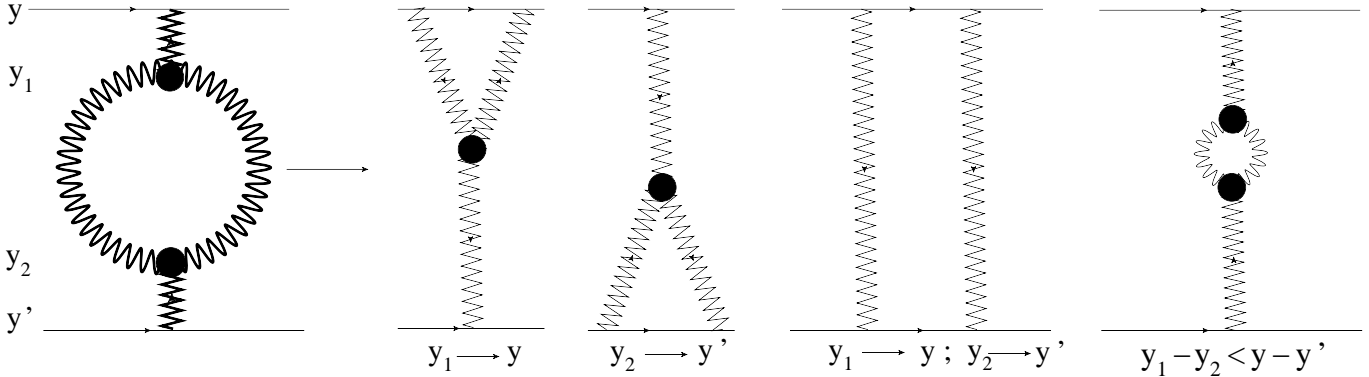


Figure 4: The first Pomeron loop diagram gives the simultaneous contribution of the fan diagram, the loop diagram and the contribution from non interacting Pomerons.

In a recent publication [8] by M. Braun, the Pomeron loop diagram was calculated using the original exact form of the triple Pomeron vertex, which was first derived by Korchemsky [1] and at the same time by Bialas, Navelet and Peschanski (BNP) in ref. [2]. It was suggested in ref. [8] that use of the Korchemsky expression for the triple Pomeron vertex, leads to a more accurate result for the Pomeron loop diagram. Therefore the approach suggested in ref. [8] has been adopted in this paper.

The approach used to find the Pomeron loop amplitude, can be extended to the calculation of more complicated diagrams (see for example Fig. 21), with an arbitrary number of Pomeron loops in the QCD approach instead of the MFA formalism. Using the new algorithm developed in this paper, the amplitude for multiple loop diagrams derives from an iterative expansion of the simple Pomeron loop amplitude. In this framework, a general formula can be found for the amplitude of the diagram with an arbitrary number of Pomeron loops in QCD, which is a function of the number of loops in the diagram, and the rapidity gap between the scattering protons. If the production of the Higgs boson is included in the diagram, the formula is also a function of the mass of the Higgs boson. This provides the mechanism for summing over Pomeron loop diagrams in the precise QCD formalism, instead of the toy model approach of ref. [5, 6]. In this approach it was found that the main contribution to the amplitude of the general enhanced diagram, is equivalent to the amplitude of the diagram with non interacting Pomerons, with renormalized Pomeron vertices.

This is a considerable step forward theoretically, since it makes possible the summation over Pomeron loop diagrams in QCD to any order. Experimentally this means that an accurate prediction for the exclusive cross section for diffractive Higgs production is possible that includes the suppression factor needed to screen out the full set of re-scattering corrections, namely the enhanced survival probability. In this new formalism it was found that the contribution of enhanced diagrams to the survival probability is substantial, confirming the results found in refs. [3, 4]. The results show also that the survival probability

is very sensitive to the choice of the strong coupling, and as such it decreases as α_s increases, in agreement with ref. [3].

This paper is organized in the following way. In section 2 the notation and conventions used throughout this paper are listed. The amplitude for the basic diagram of Fig. 7, which shows diffractive Higgs production through single t-channel Pomeron exchange is derived. Section 3 is devoted to the derivation of the amplitude of the Pomeron loop, shown in Fig. 9. A pedagogical approach is taken to explain the style of integration over the conformal variables in the loop. This forms the basis of the techniques used for more complicated diagrams in later sections. In section 4 the main idea used to derive the formula for the general multiple Pomeron loop diagram is outlined, which is an iterative technique. Using this iterative approach, in section 5, more complicated multiple Pomeron loop diagrams, such as Fig. 14, Fig. 15 and Fig. 21 are calculated. Finally in section 6 the general expression for the amplitude of the diagram with an arbitrary number of Pomeron loops is derived. This provides the tools necessary to sum over the complete set of Pomeron loop diagrams up to any order. The summation over enhanced diagrams forms the basis for section 7, to estimate the enhanced survival probability $\langle |S_{\text{enh}}^2| \rangle$. These results are discussed in the conclusion in section 8. In the appendix section a brief overview of the derivation of the triple Pomeron vertex is given, mostly following the strategy of Korchemsky in ref. [1], and the amplitude of the first fan diagram of Fig. 26 is calculated.

2. The Pomeron propagator

The following conventions and notations will be used, some of which are based on the paper of ref. [8] by M. Braun. The Pomeron propagator shown in Fig. 5, which is a t channel exchange between two color dipoles in QCD, with rapidity values y and y' , is denoted by the expression;

$$g_{y-y'} = g_{y-y'}(R, r_1, r_2 | R', r'_1, r'_2) \quad (2.1)$$

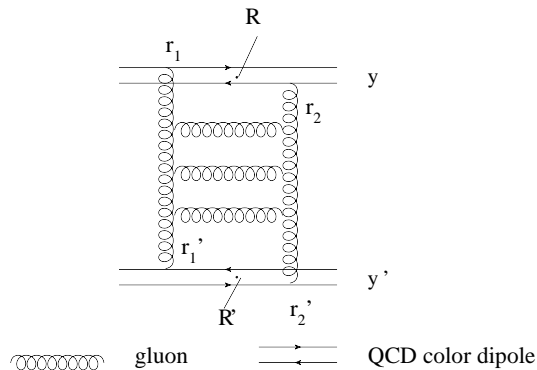


Figure 5: Coordinates for the two reggeized gluons in the BFKL Pomeron propagator, in color dipole scattering.

where as shown in Fig. 5, r_1 and r_2 denote the initial and final coordinates of the two reggeized gluons, and R is the center of mass coordinate of the two reggeized gluons. The conformally invariant expression, for the coupling of the BFKL Pomeron to the QCD color dipole is;

$$E_\gamma = \left(\frac{r_{12}}{r_{10}r_{20}} \right)^\gamma \left(\frac{r_{12}^*}{r_{10}^*r_{20}^*} \right)^{\tilde{\gamma}} \quad (2.2)$$

where $r_{ij} = r_i - r_j$ and $r_{i0} = r_i - R$. The conformal weights are given by the expression

$$\gamma = \frac{1+n}{2} + i\nu; \quad \tilde{\gamma} = 1 - \gamma^*; \quad n \in \mathbb{Z}; \quad \nu \in \mathbb{R} \quad (2.3)$$

Two important properties of the conformal weights are

$$\gamma - \tilde{\gamma} = n \quad \gamma + \tilde{\gamma} = 1 + 2i\nu \quad (2.4)$$

where n is the conformal spin, and ν is the scaling dimension of the state. Wherever γ appears, it is intended to be a shorthand for the set of two numbers $\{n, \nu\}$. The above expression for the Pomeron propagator in Eq. (2.1) can also be written in the representation of complex angular momentum $j = 1 + \omega$ instead of rapidity y by the following Mellin transformation;

$$g_{y-y'} = \int_{a-i\infty}^{a+i\infty} \frac{d\omega}{2\pi i} e^{\omega(y-y')} g_\omega \quad (2.5)$$

where in ω representation, the Pomeron propagator is given by the following expression;

$$g_\omega = \int d^2R \int d^2R' \int \mathcal{D}\gamma E_\gamma E'_{-\tilde{\gamma}} g_\omega(\gamma) \quad (2.6)$$

where $\mathcal{D}\gamma$ is a shorthand notation for

$$\int \mathcal{D}\gamma = \oint_{C_\gamma} d\gamma h(\gamma); \quad \text{where} \quad h(\gamma) = \frac{2}{\pi^4} \left| \gamma - \frac{1}{2} \right|^2 \quad (2.7)$$

The contour C_γ shown in Fig. 6 consists of the imaginary γ axis from $\pm i\infty$, and the semi circle at infinity, to the left of the imaginary γ axis. C_γ encloses all singularities in the integrand of Eq. (2.6). The integrand vanishes on the semi circle at infinity, such that it is sufficient just to replace

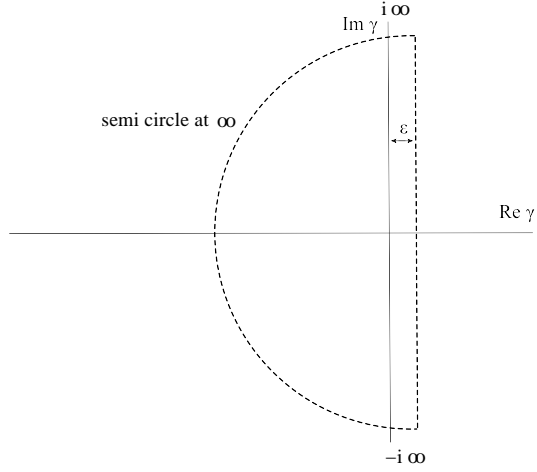


Figure 6: Contour enclosing singularities for the integration over the conformal variable γ .

The notation $\sum_{n=-\infty}^{\infty} \int_{-\infty}^{\infty} d\nu$, corresponds to the integration over the quantum numbers associated with the continuous unitary variable irreducible representations of $SL(2, \mathbb{C})$, defined in Eq. (2.3) (see refs. [9, 10, 11] for a detailed explanation). Thus in terms of ν ;

$$\int \mathcal{D}\gamma = \sum_{n=-\infty}^{\infty} \int_{-\infty}^{\infty} d\nu h(n, \nu) \quad (2.10)$$

$$\text{where} \quad h(n, \nu) = \frac{2}{\pi^4} \left| \gamma - \frac{1}{2} \right|^2 = \frac{2}{\pi^4} \left(\nu^2 + \frac{n^2}{4} \right) \quad (2.11)$$

The conformal propagator $g_\omega(\gamma)$ takes the form;

$$g_\omega(\gamma) = \frac{1}{\omega - \omega(n, \nu)} \lambda(n, \nu) \quad (2.12)$$

$$\begin{aligned} \text{where} \quad \lambda(n, \nu) &= \frac{1}{16} \times \frac{1}{h(n+1, \nu) h(n-1, \nu)} \\ &= \frac{1}{16} \frac{1}{\left\{ \nu^2 + (n+1)^2/4 \right\} \left\{ \nu^2 + (n-1)^2/4 \right\}} \end{aligned} \quad (2.13)$$

$\omega(n, \nu)$ are the eigenfunctions of the BFKL equation, which represent the energy levels of the BFKL Pomeron, and these are given by the expression

$$\oint_{C_\gamma} d\gamma \rightarrow \int_{\epsilon-i\infty}^{\epsilon+i\infty} d\gamma \quad (2.8)$$

It is more economical to calculate diagrams with BFKL Pomeron states in terms of ν , instead γ . For the integration limits $\epsilon + i\infty \leq \gamma \leq \epsilon - i\infty$ (as $\epsilon \rightarrow 0$), Eq. (2.3) gives the corresponding limits of integration for the variable ν , as $-\infty \leq \nu \leq \infty$, and one should sum over all real positive integers n . In this way in Eq. (2.6), one can replace the integration over γ with the integration over ν using the notation

$$\sum_{n=-\infty}^{\infty} \int_{\epsilon-i\infty}^{\epsilon+i\infty} d\gamma = \sum_{n=-\infty}^{\infty} \int_{-\infty}^{\infty} d\nu \quad (2.9)$$

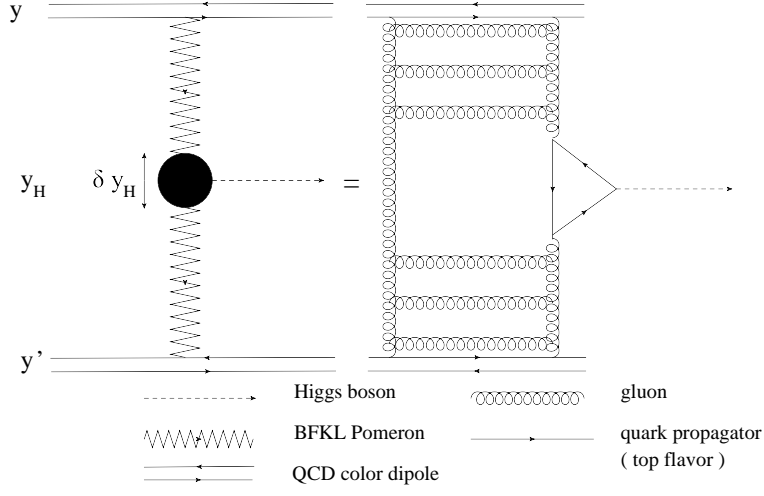


Figure 7: Diffractive production of the Higgs boson through t-channel Pomeron exchange. The process Pomeron + Pomeron \rightarrow Higgs proceeds mostly through the top quark triangle.

$$\omega(n, \nu) = \bar{\alpha}_s \{ \psi(1) - \Re e \psi(\gamma) \} = \bar{\alpha}_s \{ 2\psi(1) - \psi(\gamma) - \psi(1 - \gamma) \} \quad (2.14)$$

where the function

$$\psi(x) = \frac{d \ln \Gamma(x)}{dx} = \frac{1}{\Gamma(x)} \frac{d\Gamma(x)}{dx} \quad (2.15)$$

is the Di-gamma function, and where $\Gamma(x) = (x - 1)!$ is the Euler Gamma function. Throughout this paper, the notation

$$\bar{\alpha}_s = \frac{\alpha_s N_c}{\pi}; \quad (2.16)$$

where N_c is the number of colors in the $SU(N_c)$ color group, or abstractly speaking, N_c is the number of generators for the standard representation of $SU(N_c)$. For QCD, $N_c = 3$. Here, α_s is the strong coupling for QCD interactions, and it depends inversely on energy. Wherever a value for α_s is used in a calculation, its value for a specific choice of energy scale will be stated explicitly.

Substituting for the conformal propagator Eq. (2.12) in Eq. (2.5), and using the integration measure of Eq. (2.10) to integrate over the conformal variable, the amplitude for diffractive Higgs production through the t channel Pomeron exchange process shown in Fig. 7 is;

$$A_{(0)}(\Delta, \delta y_H | \text{Fig. 7}) = \frac{\alpha_s^2}{4} \sum_{n=-\infty}^{\infty} \int_{-\infty}^{\infty} d\nu h(n, \nu) \lambda(n, \nu) \exp\{\omega(n, \nu)(\Delta - \delta y_H)\} E_\gamma E'_{-\tilde{\gamma}'} A_H \quad (2.17)$$

where $\Delta = y - y'$ is the rapidity gap between the scattering dipoles shown in Fig. 7, and $\delta y_H = \ln(M_H^2/4s_0)$ is the window of rapidity occupied by the heavy Higgs boson (M_H is the mass of the Higgs boson and $s_0 = 1 \text{ GeV}^2$). The notation $A_{(0)}$ represents the fact that there are $N = 0$ generations of Pomeron branching, since later on the notation $A_{(N)}$ is used to label the diagram with N generations of Pomeron branching. The numerical factor of $\alpha_s^2/4$ in front of Eq. (2.17) takes into account the couplings of the two reggeized gluons in the BFKL Pomeron structure in Fig. 7, to the color dipoles. Since there are two gluons which each couple twice at both ends to the QCD color dipole, this leads to a factor which is proportional to α_s^2 . The factor of $1/4$ accounts for the 4 degenerate diagrams in Fig. 7, which arise due to the different ways of coupling the reggeized gluons to the color dipoles. Hence one divides by a symmetry factor which ensures that identical diagrams are only counted once. A more detailed explanation of this coefficient can be found in refs. [9, 10, 12]. A_H in Eq. (2.17) represents the amplitude for the subprocess where Pomeron + Pomeron \rightarrow Higgs, which is given by the expression [13, 14, 15, 16, 17, 18]

$$\begin{aligned} A_H &= \frac{1}{3} \frac{2^{1/4} G_F^{1/2} \alpha_s(M_H)}{\pi} (N_c^2 - 1) \quad (G_F = 1.166 \times 10^{-5} \text{ GeV}^{-2}) \\ &= 6.89 \times 10^{-4} \text{ GeV}^{-2} \end{aligned} \quad (2.18)$$

where G_F is the Fermi constant. Here a typical value for α_s , at the scale of M_Z , the mass of the Z boson, is used. It is expected that the Higgs will be produced with a mass of approximately $100 \text{ GeV}/c^2$, which would give a value for the strong coupling constant $\alpha_s \sim 0.12$. This corresponds to a Z particle mass [19], of $M_Z = 90.8 \pm 0.6 \text{ GeV}/c^2$. The leading order contribution to this process is where one of the two reggeized gluons in the BFKL Pomeron states produces the Higgs boson through the quark triangle shown in Fig. 7, for which the top flavour dominates. This is on account of the quark + quark \rightarrow Higgs vertex in Fig. 7 which is proportional to the mass of the quark flavour, so the top flavour which is the heaviest ($m_{\text{top}} = 175 \text{ GeV}/c^2$) contributes the most.

The BFKL eigenfunction specified in Eq. (2.14) decreases sharply as n decreases. In fact, the BFKL eigenfunction remains positive at high energy, only when $n = 0$. For this reason, solutions with $n \neq 0$ are negligible, and from here onwards will be ignored. Note that from the definition of Eq. (2.14) in the case when $n = 0$;

$$\omega(\nu) = \bar{\alpha}_s \left\{ 2\psi(1) - \psi\left(\frac{1}{2} + i\nu\right) - \psi\left(\frac{1}{2} - i\nu\right) \right\} \quad (2.19)$$

which has a saddle point at $\nu = 0$. Hence for the BFKL eigenfunction one can use the expansion around the point $\nu = 0$

$$\omega(\nu) = \omega(0) - \frac{1}{2}\nu^2\omega''(0) + \mathcal{O}(\nu^3) \quad (2.20)$$

so that Eq. (2.17) simplifies to

$$A_{(0)}(\Delta, \delta y_H | \text{Fig. 7}) = \frac{\alpha_s^2}{2\pi^4} \int_{-\infty}^{\infty} d\nu \frac{\nu^2}{(1+4\nu^2)^2} \times \exp \left\{ \omega(0)(\Delta - \delta y_H) - \frac{1}{2}\nu^2\omega''(0)(\Delta - \delta y_H) + i\nu \ln(E E') \right\} A_H \quad (2.21)$$

$$\text{where } E = \left(\frac{r_{12}}{r_{10}r_{20}} \right) \left(\frac{r_{12}}{r_{10}r_{20}} \right)^* ; \quad E' = \left(\frac{r'_{12}}{r'_{10}r'_{20}} \right) \left(\frac{r'_{12}}{r'_{10}r'_{20}} \right)^* \quad (2.22)$$

The integration over ν in Eq. (2.21) can be solved by using the method of steepest descents. In this technique the exponential is expanded around the saddle point ν_{sp} (in this case $\nu_{sp} = \ln(E E') / \omega''(0)(\Delta - \delta y_H)$) and the remaining part of the integrand is fixed by setting the integration variable $\nu = \nu_{sp}$. In this way the integration reduces to a Gaussian type integration over ν , and using the result that $\int_{-\infty}^{\infty} dx x^2 e^{-ax^2} = \pi^{1/2}/2 \times a^{-3/2}$ ($a \neq 0$), Eq. (2.21) yields the result;

$$A_{(0)}(\Delta, \delta y_H | \text{Fig. 7}) = \frac{\alpha_s^2 \pi^{1/2}}{4\pi^4} \left(\frac{2}{\omega''(0)(\Delta - \delta y_H)} \right)^{3/2} \exp \left\{ \omega(0)(\Delta - \delta y_H) - \frac{\ln^2(E E')}{2\omega''(0)(\Delta - \delta y_H)} \right\} \times \left(1 + \mathcal{O} \left(\frac{\ln(E E')}{\omega''(0)(\Delta - \delta y_H)} \right) \right) A_H \quad (2.23)$$

In the case where the ν saddle point $\nu_{sp} = \ln(E E') / (\omega''(0)(\Delta - \delta y_H))$ is small, then one can recast Eq. (2.23) in the following asymptotic form, namely

$$A_{(0)}(\Delta, \delta y_H | \text{Fig. 7}) = \frac{(2\pi)^{1/2} \bar{\alpha}_s^2 A_H}{2\pi^2 N_c^2} \frac{e^{\omega(0)(\Delta - \delta y_H)}}{(\omega''(0)(\Delta - \delta y_H))^{3/2}} \\ = 1.57 \times 10^{-8} \text{ GeV}^{-2} \quad (\alpha_s = 0.12) \\ = 2.17 \times 10^{-7} \text{ GeV}^{-2} \quad (\alpha_s = 0.2) \quad (2.24)$$

The following values were used;

$$\omega(0) = 4\bar{\alpha}_s \ln 2; \quad \omega''(0) = 28\bar{\alpha}_s \zeta(3); \\ \Delta = 19; \quad \delta y_H = \ln \left(\frac{M_H^2}{4s_0} \right) \\ = 7.824 \quad (2.25)$$

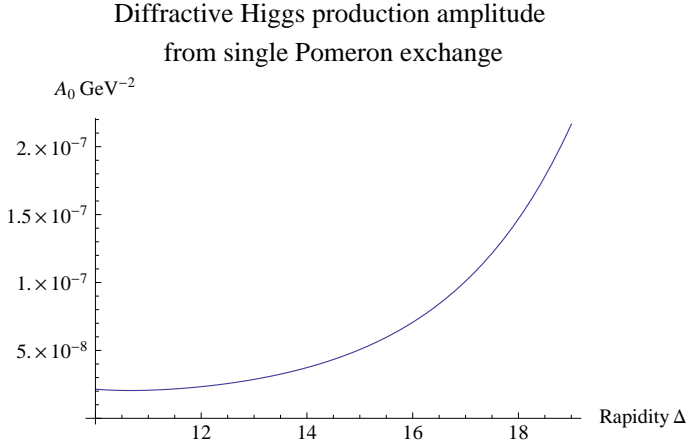


Figure 8: Plot of $A_{(0)}(\Delta, \delta y_H)$ (Fig. 7) derived in Eq. (2.24) against the rapidity gap Δ between the scattering dipoles. The values for the rapidity gap Δ go from $\delta y_H = \ln(M_H^2/4s_0)$ for the Higgs mass $M_H = 100$ GeV and $s_0 = 1$ GeV², up to the typical LHC rapidity $\Delta = 19$.

3. The simple Pomeron loop

In this section, the Feynman amplitude for the diffractive production of the Higgs boson, from the Pomeron loop diagram is derived. The diagram shown in Fig. 9 is the scattering of a color dipole at rapidity y off a color dipole at rapidity y' , with the exchange of a BFKL Pomeron state, where the correction of one loop is included. Its amplitude is denoted $A_{(1)}(\omega, \omega', \omega_1)$, since there is one generation of Pomeron splitting, and likewise one generation of recombining of two Pomerons into one, to form the loop.

$$A_{(1)}(\omega, \omega', \omega_1 | \text{Fig. 9}) = \frac{\alpha_s^2}{4} \int \mathcal{D}\gamma \int \mathcal{D}\gamma' E_\gamma E'_{-\tilde{\gamma}'} g_\omega(\gamma) g_{\omega'}(\gamma') D_{(1)}(\gamma, \gamma' | \omega, \omega_1) A_H \quad (3.1)$$

The contribution $D_{(1)}(\gamma, \gamma' | \omega, \omega_1)$ of the Pomeron loop to the amplitude of Fig. 9, is written in ω representation as a function of the two conformal weights γ and γ' of the Pomeron propagators attached to the loop, namely;

$$D_{(1)}(\gamma, \gamma' | \omega, \omega_1) = \int d^2 R \int d^2 R' d_{(1)}(\gamma, \gamma' | \omega, \omega_1) \quad (3.2)$$

where R and R' are the center of mass coordinates of the two Pomeron propagators on either side of the loop, and

where $\zeta(n)$ is the Riemann-zeta function, and where the rapidity gap Δ between the scattering dipoles is based on the energy $\sqrt{s} = 14$ TeV, which is typical for proton collisions at the LHC. The values given in Eq. (2.25) will be assumed throughout this paper. The difference in the values of Eq. (2.24) shows that the amplitude depends critically on the choice of the strong coupling. The plot of the single Pomeron amplitude derived in Eq. (2.24) against rapidity is shown in Fig. 8, for $\alpha_s = 0.2$. The plot shows that the amplitude of Fig. 7 is very sensitive to increases in the rapidity gap Δ .

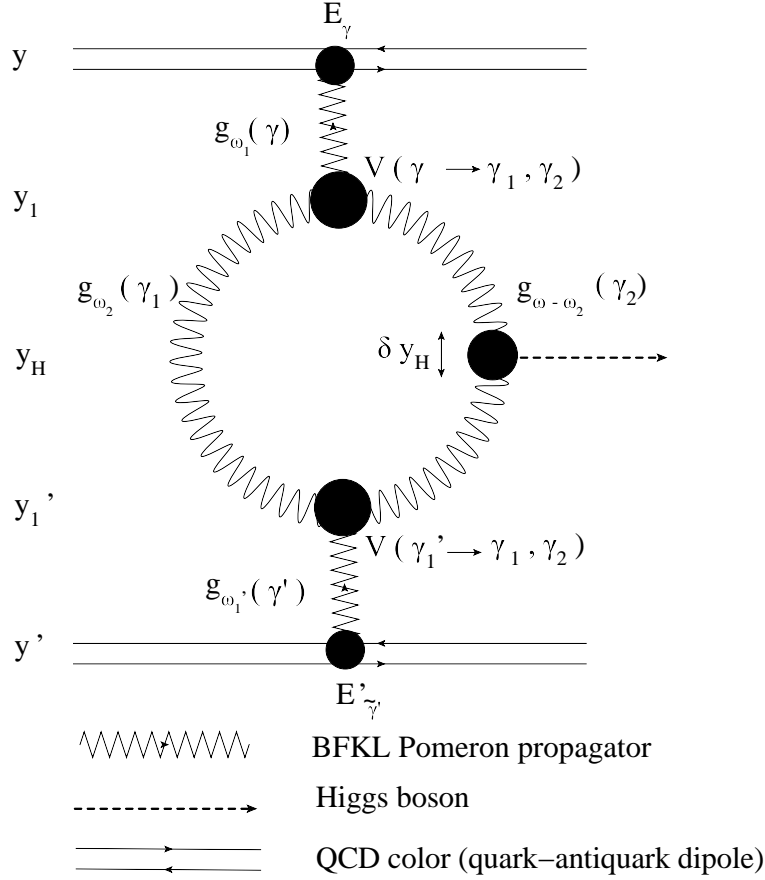


Figure 9: The Pomeron loop diagram.

$$\begin{aligned}
d_{(1)}(\gamma, \gamma' | \omega, \omega_1) &= \frac{1}{S_{(1)}} \int d^2 R_1 \int d^2 R_2 \int \mathcal{D}\gamma_1 \int \mathcal{D}\gamma_2 g_{\omega_1}(\gamma_1) g_{\omega_2}(\gamma_2) \\
&\quad \times V(R, R_1, R_2 | \gamma \rightarrow \gamma_1, \gamma_2) V(R', R_1, R_2 | \gamma_1, \gamma_2 \rightarrow \gamma')
\end{aligned} \tag{3.3}$$

$S_{(1)}$ in the denominator is a symmetry factor which prevents counting identical diagrams more than once, and its value is determined below. $V(R, R_1, R_2 | \gamma \rightarrow \gamma_1, \gamma_2)$ is the vertex for the splitting of the BFKL Pomeron state labeled $\{R, \gamma\}$, into the two BFKL Pomeron states labeled by $\{R_1, \gamma_1\}$ and $\{R_2, \gamma_2\}$, and it is known as the triple Pomeron vertex, shown in Fig. 10, ($\gamma =$ conformal variable and $R =$ center of mass coordinate).

The total order of the symmetry group of Fig. 9 is $S_{(1)} = 16$. This can be seen by observing that for both vertices of the loop, there are 2 permutations of the Pomeron lines which form the 2 branches of the loop. In addition for each pair of Pomeron lines there are 2 permutations formed by swapping the upper

with the lower vertex. This makes a total symmetry factor of 4. The remaining 4-fold degeneracy stems from the triple Pomeron vertex shown in Fig. 10, whereby swapping the reggeized gluon lines (5) and (6) leads to an identical diagram. However swapping lines (3) and (4) leads to two different diagrams called the planar and non-planar diagrams shown in Fig. 11 and Fig. 12. These two diagrams are non identical, and give different contributions, where the latter is suppressed by $1/N_c^2$.

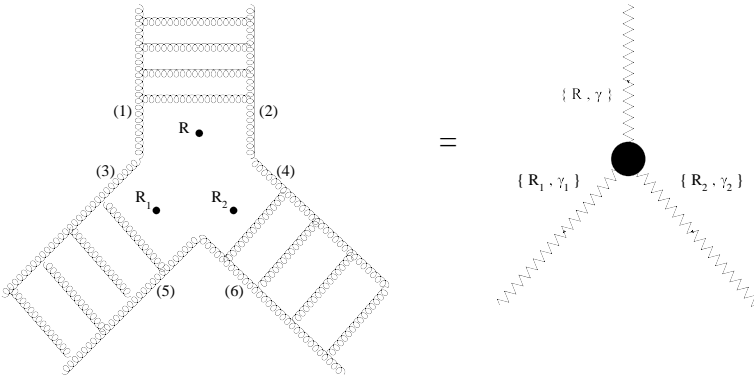


Figure 10: The triple Pomeron vertex.

Korchemsky pointed out in ref. [1], that by the condition of conformal invariance, the triple Pomeron vertex can be factorized into two pieces which depend only on the center of mass coordinates, and the conformal variables respectively, in the following way;

$$V(R, R_1, R_2 | \gamma \rightarrow \gamma_1, \gamma_2) = R_{01}^{-\Delta_{01}} R_{12}^{-\Delta_{12}} R_{20}^{-\Delta_{20}} R_{01}^{*-\tilde{\Delta}_{01}} R_{12}^{*-\tilde{\Delta}_{12}} R_{20}^{*-\tilde{\Delta}_{20}} \Gamma(\gamma | \gamma_1, \gamma_2) \quad (3.4)$$

where $R_{0i} = R - R_i$ ($i = 1, 2$) and $R_{12} = R_1 - R_2$, and where for example $\Delta_{01} = \gamma + \gamma_1 - \gamma_2$, and $\Delta_{12} = \gamma_1 + \gamma_2 - \gamma$, with an equivalent definition for the $\tilde{\Delta}$ in terms of the $\tilde{\gamma}$. It was found in refs. [1, 2] that;

$$\Gamma(\gamma | \gamma_1, \gamma_2) = \left(\frac{\alpha_s N_c}{\pi} \right)^2 16 \gamma (1 - \gamma) \tilde{\gamma} (1 - \tilde{\gamma}) \times \left\{ \underbrace{\Omega(\gamma | \gamma_1, \gamma_2)}_{\text{planar piece Fig. 11}} + \underbrace{\frac{2\pi}{N_c^2} \Lambda(\gamma | \gamma_1, \gamma_2) (\chi(\gamma_1) + \chi(\gamma_2) - \chi(\gamma))}_{\text{non-planar piece Fig. 12}} \right\} \quad (3.5)$$

$$\text{where } \chi(\gamma) = \Re \{ \psi(1) - \psi(\gamma) \} \quad (3.6)$$

where $\psi(\gamma)$ is the di-gamma function. The triple Pomeron vertex comes in two types, namely the planar and the non planar diagram shown in Fig. 11 and Fig. 12 respectively. The first term in curly brackets is the contribution of the planar diagram, and the second term is the contribution of the non planar diagram. The explicit expressions for $\Omega(\gamma | \gamma_1, \gamma_2)$ and $\Lambda(\gamma | \gamma_1, \gamma_2)$ and their derivation, can be found in the appendix.

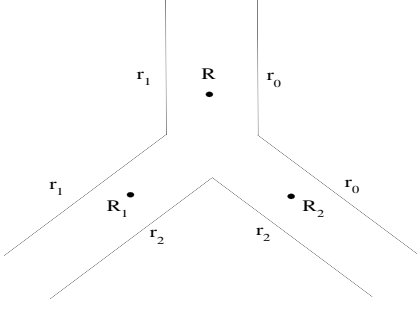


Figure 11: Planar diagram [1].

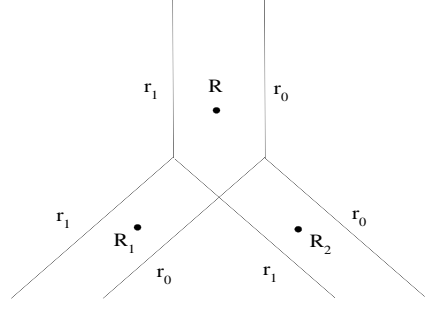


Figure 12: Non planar diagram [1].

By inserting Eq. (3.4) into Eq. (3.3) and evaluating all the integrals over the center of mass coordinates, it was shown in ref. [8] that this leads to the following condition;

$$d_{(1)}(\gamma, \gamma' | \omega, \omega_1) = d_{(1)}(\gamma | \omega, \omega_1) \frac{1}{h(\gamma)} \delta_{n,n'} \delta(\nu - \nu') \delta^{(2)}(R - R') \quad (3.7)$$

$$\text{where} \quad d_{(1)}(\gamma | \omega, \omega_1) = \frac{1}{16} \int \mathcal{D}\gamma_1 \int \mathcal{D}\gamma_2 g_{\omega_1}(\gamma_1) g_{\omega - \omega_1}(\gamma_2) \Gamma(\gamma | \gamma_1, \gamma_2) \Gamma(\bar{\gamma} | \bar{\gamma}_1, \bar{\gamma}_2) \quad (3.8)$$

Now inserting the loop amplitude of Eq. (3.8) into the scattering amplitude of Eq. (3.1), the integration over γ' can be eliminated by virtue of the Dirac delta function $\delta(\gamma - \gamma')$. Hence after introducing the explicit expressions for the integration measure and the conformal propagator given by Eq. (2.10) and Eq. (2.12) respectively;

$$\begin{aligned} A_{(1)}(\omega, \omega', \omega_1 | \text{Fig. 9}) &= \frac{\alpha_s^2}{4} \int \mathcal{D}\gamma \frac{\lambda^2(\gamma)}{\{\omega - \omega(\gamma)\} \{\omega' - \omega(\gamma)\}} E_\gamma E'_{-\bar{\gamma}} A_H \\ &\times \frac{1}{16} \int \mathcal{D}\gamma_1 \int \mathcal{D}\gamma_2 \frac{\lambda(\gamma_1)}{\{\omega - \omega(\gamma_1)\}} \frac{\lambda(\gamma_2)}{\{\omega - \omega_1 - \omega(\gamma_2)\}} \Gamma(\gamma | \gamma_1, \gamma_2) \Gamma(\bar{\gamma} | \bar{\gamma}_1, \bar{\gamma}_2) \end{aligned} \quad (3.9)$$

The amplitude of the Pomeron loop diagram can be re-expressed as a function of the rapidity instead of the angular momentum $j = 1 + \omega$, using the Mellin transform. The rapidity gap filled up by the loop is $\Delta_1 = y_1 - y'_1$, where y_1 and y'_1 are respectively the rapidity values of the upper and lower vertices of the loop (see Fig. 9). In the case of inelastic scattering which results in the production of the heavy Higgs boson from one branch of the loop, there will be a window of rapidity δy_H which the Higgs boson occupies. Therefore δy_H should be the minimum rapidity gap which the loop occupies, such that the energy of the scattering is enough to produce the Higgs boson. This affects the upper and lower limits of the rapidity variables y_1 and y'_1 , and hence the choice of integration limits are as they appear below in Eq. (3.10);

$$\begin{aligned}
A_{(1)}(\Delta, \delta y_H | \text{Fig. 9}) &= \int_{y'+\delta y_H}^y dy_1 \int_{y'}^{y_1-\delta y_H} dy'_1 \\
&\times \int \frac{d\omega}{2\pi i} e^{\omega(y-y_1)} \int \frac{d\omega'}{2\pi i} e^{\omega'(y'_1-y')} \int \frac{d\omega_1}{2\pi i} e^{\omega_1(y_1-y'_1)} A_{(1)}(\omega, \omega', \omega_1 | \text{Fig. 9}) \\
&= \frac{\alpha_s^2}{4} \int \mathcal{D}\gamma \lambda^2(\gamma) e^{\omega(\gamma)\Delta} d_{(1)}(\gamma | \Delta, \delta y_H) E_\gamma E'_{-\bar{\gamma}} A_H
\end{aligned} \tag{3.10}$$

where $\Delta = y - y'$ is the rapidity gap between the scattering dipoles. The loop amplitude in rapidity representation is given by the expression;

$$\begin{aligned}
d_{(1)}(\gamma | \Delta, \delta y_H) &= \frac{1}{16} \int \mathcal{D}\gamma_1 \int \mathcal{D}\gamma_2 \lambda(\gamma_1) \lambda(\gamma_2) \Gamma(\gamma | \gamma_1, \gamma_2) \Gamma(\bar{\gamma} | \bar{\gamma}_1, \bar{\gamma}_2) \\
&\times \int_{y'+\delta y_H}^y dy_1 \int_{y'}^{y_1-\delta y_H} dy'_1 \exp \{ (\omega(\gamma_1) + \omega(\gamma_2) - \omega(\gamma)) (y_1 - y'_1) - \omega(\gamma_1) \delta y_H \}
\end{aligned} \tag{3.11}$$

Assuming that the leading contribution at high energy stems from the region where the conformal spins $n = n_1 = n_2 = 0$, and introducing the explicit expressions given in Eq. (2.10), Eq. (2.11) and Eq. (2.13) for the integration measure and the conformal propagator, the scattering amplitude of Eq. (3.10) reduces to

$$A_{(1)}(\Delta, \delta y_H | \text{Fig. 9}) = \frac{\alpha_s^2}{4} \int_{-\infty}^{\infty} d\nu h(\nu) \lambda^2(\nu) e^{\omega(\nu)\Delta} d_{(1)}(\nu | \Delta, \delta y_H) E_\nu E'_{-\nu} A_H \tag{3.12}$$

where (when the conformal spins $n_1 = n_2 = 0$) the loop amplitude simplifies to;

$$\begin{aligned}
d_{(1)}(\nu | \Delta, \delta y_H) &= \frac{1}{2^{10}\pi^8} \int_{-\infty}^{\infty} d\nu_1 \int_{-\infty}^{\infty} d\nu_2 \frac{\nu_1^2}{(\nu_1^2 + 1/4)^2} \frac{\nu_2^2}{(\nu_2^2 + 1/4)^2} \left| \Gamma(\nu | \nu_1, \nu_2) \right|^2 \\
&\times \int_{y'+\delta y_H}^y dy_1 \int_{y'}^{y_1-\delta y_H} dy'_1 \exp \{ (\omega(\nu_1) + \omega(\nu_2) - \omega(\nu)) (y_1 - y'_1) - \omega(\nu_1) \delta y_H \}
\end{aligned} \tag{3.13}$$

A convention used in Eq. (3.13) and throughout this paper, is that wherever ν appears alone without n , it has been assumed that $n = 0$ and it has been suppressed. For example $\Gamma(\gamma | \gamma_1, \gamma_2)_{n=n_1=n_2=0}$ is labeled $\Gamma(\nu | \nu_1, \nu_2)$, and $\omega(n=0, \nu)$ is labeled $\omega(\nu)$. In the region where $n = n_1 = n_2 = 0$, then $\Gamma(\bar{\gamma} | \bar{\gamma}_1, \bar{\gamma}_2)_{n=n_1=n_2=0} \equiv \Gamma(-\nu | -\nu_1, -\nu_2)$, and hence in Eq. (3.13), the notation $\left| \Gamma(\nu | \nu_1, \nu_2) \right|^2 = \Gamma(\nu | \nu_1, \nu_2) \Gamma(\nu | \nu_1, \nu_2)^* \equiv \Gamma(\nu | \nu_1, \nu_2) \Gamma(-\nu | -\nu_1, -\nu_2)$.

Two main regions are considered when evaluating the $\{\nu, \nu_1, \nu_2\}$ integrals of Eq. (3.12) and Eq. (3.13). Region I is $\{\nu, |\nu_1|, |\nu_2|\} = \{0, 1/2, 1/2\}$ and region II is $\{|\nu|, \nu_1, \nu_2\} = \{1/2, 0, 0\}$. To find the contribution from region I, after integrating over the rapidity variables y_1 and y'_1 , the loop amplitude of Eq. (3.13) takes the form;

$$\begin{aligned}
d_{(1)}^I(\nu | \Delta, \delta y_H) &= \frac{e^{-\omega(\nu)\delta y_H}}{2^{10}\pi^8} \int_{-\infty}^{\infty} d\nu_1 \int_{-\infty}^{\infty} d\nu_2 \frac{\nu_1^2}{(\nu_1^2 + 1/4)^2} \frac{\nu_2^2}{(\nu_2^2 + 1/4)^2} \left| \Gamma(\nu | \nu_1, \nu_2) \right|^2 \\
&\times e^{\omega(\nu_2)\delta y_H} \int_0^{\infty} d\beta e^{(\omega(\nu) - \omega(\nu_1) - \omega(\nu_2))\beta} \\
&\times \left(\Delta - \delta y_H + \beta - \beta e^{(\omega(\nu_1) + \omega(\nu_2) - \omega(\nu))(\Delta - \delta y_H)} \right)
\end{aligned} \tag{3.14}$$

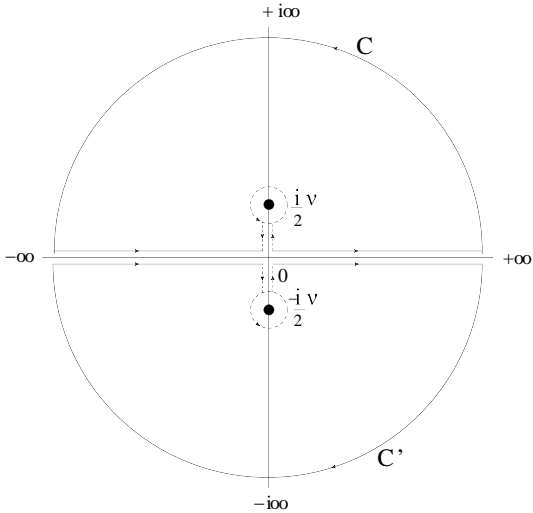


Figure 13: The integration contour C (C') which is closed on the upper (lower) half plane, in order to enclose the pole $i\nu = 1/2$ ($-1/2$).

where in Eq. (3.14) the identity $1/x^n = 1/\Gamma(n) \times \int_0^{\infty} d\beta e^{-\beta x} \beta^{n-1}$ has been used. The singularities in the integrand at $\{|\nu_1|, |\nu_2|\} = 1/2$ suggest closing the ν_1 and ν_2 integration paths along the contour C (or C') shown in Fig. 13 which runs along the real axis from $-\infty$ to $+\infty$ and along the semi circle at infinity in the upper (lower) half plane. C (C') encloses the points $\{i\nu_1, i\nu_2\} = 1/2$ ($-1/2$), and the two solutions which stem from both contours are identical. Therefore the contour C is chosen, so that the solution is $2 \times (2\pi i)^2 \sum$ (residues at $\{i\nu_1, i\nu_2\} = 1/2$), where the extra factor of 2 takes into account the identical contribution from the residues at $\{i\nu_1, i\nu_2 = -1/2\}$. The non-singular part of the integrand of Eq. (3.14), namely $(1/2 + i\nu_1)^{-2} (1/2 + i\nu_1)^{-2}$ tends to zero as $1/\nu_1^2 \nu_2^2$, hence the convergence on the semi-circle at infinity is satisfied, allowing C to be used as the integration contour. This choice of contour will be used repeatedly in similar calculations

throughout this paper, therefore wherever a specified integration contour is labeled C , it is assumed that the path shown in Fig. 13 is intended, and that the non-singular part of the integrand has a good convergence on C .

The triple Pomeron vertex in region I which should be inserted into Eq. (3.14) is derived in the appendix in Eq. (A.22). After taking into account all the singularities that stem from Eq. (A.22) at $\{i\nu_1, i\nu_2\} = 1/2$, and the singularities that stem from $\omega(i\nu_{1,2} \rightarrow 1/2) = \bar{\alpha}_s / (1/2 - i\nu_{1,2})$ and $\chi(i\nu_{1,2} \rightarrow 1/2) = 1 / (1/2 - i\nu_{1,2})$ (see Eq. (2.19) and Eq. (3.6)), the integration over ν_1 in Eq. (3.14) takes the form;

$$\begin{aligned}
& \oint_C d\nu_1 \frac{\nu_1^2}{(1/2 + i\nu_1)^2 (1/2 - i\nu_1)^4} \exp \left\{ \frac{\bar{\alpha}_s}{(1/2 - i\nu_1)} \beta \right\} \\
&= \oint_C d\nu_1 \frac{\nu_1^2}{(1/2 + i\nu_1)^2 (1/2 - i\nu_1)^2} \left(\frac{1}{\bar{\alpha}_s} \frac{d}{d\beta} \right)^2 \exp \left\{ \frac{\bar{\alpha}_s}{(1/2 - i\nu_1)} \beta \right\}; \quad (3.15)
\end{aligned}$$

where the derivative acts on the exponential to bring down a factor of $(1/2 - i\nu_1)^{-2}$. The $(1/2 - i\nu_1)^{-2}$ term remaining is canceled by the Jacobian of the coordinate transformation $u = \bar{\alpha}_s (1/2 - i\nu_1)^{-1} + \bar{\alpha}_s (1/2 - i\nu_2)^{-1} - \omega(\nu_2) \delta y_H / \beta$, for which the Jacobian is $|\partial u / \partial \nu_1| = (1/2 - i\nu_1)^2 / \bar{\alpha}_s$. Instead integrating over u yields an integration of the form $\oint_C du \exp(-iu\beta) \equiv \pi i \delta(\beta)$ or $\oint_C du \exp(-iu(\beta - \Delta + \delta y_H)) \equiv 2\pi i \delta(\beta - \Delta + \delta y_H)$. After taking the residue at $i\nu_1 = 1/2$, the integration over ν_2 has now reduced to;

$$\begin{aligned}
& \oint_C d\nu_2 \frac{\nu_2^2 (1 - i\nu_1 - i\nu_2 - 2/N_c^2)}{(1/2 + i\nu_2)^2 (1/2 - i\nu_2)^4} \xrightarrow{i\nu_1 \rightarrow 1/2} \oint_C d\nu_2 f(\nu_2) \left(\frac{1}{(1/2 - i\nu_2)^3} - \frac{2/N_c^2}{(1/2 - i\nu_2)^4} \right) \\
&= 2\pi i \left(\frac{(-1)^2}{2!} f^{(2)}(i\nu_2 = 1/2) - \frac{2}{N_c^2} \frac{(-1)^3}{3!} f^{(3)}(i\nu_2 = 1/2) \right) \\
&= \frac{2\pi i}{4} \left(1 - \frac{2}{N_c^2} \right); \quad \text{where} \quad f(\nu_2) = \frac{\nu_2^2}{(1/2 + i\nu_2)^2} \quad (3.16)
\end{aligned}$$

Overall using the above described method for taking the integrals over ν_1 and ν_2 , and evaluating the integration over β , the loop amplitude of Eq. (3.14) becomes;

$$d_{(1)}^I(\nu|\Delta, \delta y_H) = d \left(\frac{1}{2} + i\nu \right)^3 \left(\frac{1}{2} - i\nu \right)^3 \chi(\nu) \left\{ \omega(\nu) + \frac{1}{2} \omega^2(\nu) (\Delta - \delta y_H) \right\} e^{-\omega(\nu) \delta y_H} \quad (3.17)$$

$$\text{where} \quad d = \bar{\alpha}_s \left(1 - \frac{1}{N_c^2} \right) \left(1 - \frac{2}{N_c^2} \right) \quad (3.18)$$

Now inserting the result for the loop amplitude of Eq. (3.17) into the scattering amplitude of Eq. (3.12), the steepest descent method described in section 2 can be used for the ν integration in Eq. (3.12), so that overall the contribution to the scattering amplitude which stems from the region $\{\nu, |\nu_1|, |\nu_2|\} = \{0, 1/2, 1/2\}$ is;

$$A_{(1)}^I(\Delta, \delta y_H | \text{Fig. 9}) = \frac{(2\pi)^{1/2} \bar{\alpha}_s^2 d A_H}{128\pi^2 N_c^2} \frac{e^{\omega(0)(\Delta - \delta y_H)}}{(\omega''(0)(\Delta - \delta y_H))^{3/2}} \chi(0) \left\{ \omega(0) + \frac{1}{2} \omega^2(0) (\Delta - \delta y_H) \right\} \quad (3.19)$$

$$\begin{aligned}
&= 2.34 \times 10^{-11} \text{ GeV}^{-2} \quad (\alpha_s = 0.12) \\
&1.3 \times 10^{-9} \text{ GeV}^{-2} \quad (\alpha_s = 0.2) \quad (3.20)
\end{aligned}$$

The results of Eq. (3.20) show that the Pomeron loop in region I is small compared with the basic diagram of Fig. 7 (see Eq. (2.24)). It turns out that the dominant contribution to the Pomeron loop amplitude stems from region II, namely $\{|\nu|, \nu_1, \nu_2\} = \{1/2, 0, 0\}$. In this region the expansion of Eq. (2.20) for the BFKL eigenfunctions $\omega(\nu_1)$ and $\omega(\nu_2)$ in Eq. (3.13) can be used. The triple Pomeron vertex of Eq. (A.23) derived in the appendix for region II should be inserted into Eq. (3.13). The expression of Eq. (A.23) is novel for the following reason. From Eq. (3.5) the triple Pomeron vertex in region II takes the following form [1] ($n = n_1 = n_2 = 0$ at high energy);

$$\begin{aligned} \Gamma(|\nu||\nu_1, \nu_2) (\text{region II}) &= \Gamma\left(\frac{1}{2}|0, 0\right) = 16 \left(\frac{\alpha_s N_c}{\pi}\right)^2 \\ &\times \lim_{i\nu \rightarrow 1/2} \left(\frac{1}{2} + i\nu\right)^2 \left(\frac{1}{2} - i\nu\right)^2 \left\{ \underbrace{\Omega\left(\frac{1}{2}|0, 0\right)}_{\text{planar piece Fig. 11}} + \underbrace{\frac{2\pi}{N_c^2} \Lambda\left(\frac{1}{2}|0, 0\right) \left(\chi\left(i\nu \rightarrow \frac{1}{2}\right) - 2\chi(0)\right)}_{\text{non-planar piece Fig. 12}} \right\} \end{aligned} \quad (3.21)$$

$\Omega(\frac{1}{2}|0, 0)$ and $\Lambda(\frac{1}{2}|0, 0)$ were calculated in the appendix (see Eq. (A.11) and Eq. (A.15)) and they both have a second order pole at $i\nu = 1/2$, canceled by the $(1/2 - i\nu)^2$ term in front in Eq. (3.21). However an extra pole from the non planar piece arises due to the singularity which stems from $\chi(i\nu \rightarrow 1/2) \rightarrow (1/2 - i\nu)^{-1}$ (see Eq. (3.6)). Therefore overall for region II the divergent part of the triple Pomeron vertex stems from the non planar piece, and the contribution from the planar piece is non-singular. Hence a remarkable feature of the Pomeron loop arises which has not been taken into account before, namely that the dominant contribution to the Pomeron loop amplitude comes from the non planar piece $\Lambda(|\nu|, \nu_1, \nu_2)$ of the triple Pomeron vertex shown in Fig. 12. This property has been so far ignored because previous publications assumed that $N_c \rightarrow \infty$, and since in Eq. (3.21) the non planar piece is suppressed by $2\pi/N_c^2$ compared to the planar piece, it was neglected. Taking this into account and after evaluating the ν_1 and ν_2 integrations in Eq. (3.13) using the method of steepest descents, the contribution of region II ($\{|\nu|, \nu_1, \nu_2\} = \{1/2, 0, 0\}$) to the loop of Fig. 9 simplifies to;

$$d_{(1)}^{\text{II}}(\nu | \Delta, \delta y_H) = \frac{a e^{-\omega(0) \delta y_H}}{(1/2 + i\nu)(1/2 - i\nu)} \int_{y'+\delta y_H}^y dy_1 \int_{y'}^{y_1 - \delta y_H} dy_1' \frac{e^{(2\omega(0) - \omega(\nu))\Delta_1}}{\Delta_1^{3/2} (\Delta_1 - \delta y_H)^{3/2}} \quad (3.22)$$

$$\text{where } a = \frac{2^9 \bar{\alpha}_s^4}{N_c^4 \pi [\omega''(0)]^3}; \quad \Delta_1 = y_1 - y_1'. \quad (3.23)$$

Inserting Eq. (3.22) into Eq. (3.12), taking into account the singularities that stem from $\omega(i\nu \rightarrow 1/2) \rightarrow (1/2 - i\nu)^{-1}$ (see Eq. (2.19)) and closing the contour of integration on the path C shown in Fig. 13, the ν integration takes the form;

$$\begin{aligned}
& \oint_C d\nu \frac{\nu^2}{(1/2 + i\nu)^5 (1/2 - i\nu)^5} \exp \left\{ \frac{\bar{\alpha}_s (\Delta - \Delta_1)}{1/2 - i\nu} \right\} \\
&= \oint_C d\nu \frac{\nu^2}{(1/2 + i\nu)^5 (1/2 - i\nu)^2} \left(\frac{-1}{\bar{\alpha}_s} \frac{d}{d\Delta} \right)^3 \exp \left\{ \frac{\bar{\alpha}_s (\Delta - \Delta_1)}{1/2 - i\nu} \right\} \quad (3.24)
\end{aligned}$$

The remaining $(1/2 - i\nu)^{-2}$ term is canceled by the Jacobian of the transformation $u = \bar{\alpha}_s / (1/2 - i\nu)$, and integrating over u yields the derivative of the Dirac delta function $2\pi i \delta^3(\Delta - \Delta_1) / \bar{\alpha}_s^3$, which is absorbed by the integration over the rapidity variables $\{y_1, y_1'\}$ in Eq. (3.12). Overall the contribution of region II ($\{|\nu|, \nu_1, \nu_2\} = \{1/2, 0, 0\}$) to the scattering amplitude of Fig. 9 is;

$$A_{(1)}^{\text{II}}(\Delta, \delta y_H | \text{Fig. 9}) = \frac{\bar{\alpha}_s a A_H}{2^9 N_c^2 \pi} (\Delta - \delta y_H) \left(\frac{-1}{\bar{\alpha}_s} \frac{d}{d\Delta} \right)^3 \left\{ \frac{e^{2\omega(0)(\Delta - \delta y_H/2)}}{\Delta^{3/2} (\Delta - \delta y_H)^{3/2}} \right\} \quad (3.25)$$

$$\begin{aligned}
&= 2.05 \times 10^{-10} \text{ GeV}^{-2} & (\alpha_s = 0.12) \\
&2.14 \times 10^{-7} \text{ GeV}^{-2} & (\alpha_s = 0.2) \quad (3.26)
\end{aligned}$$

An obvious divergence in the integrand of Eq. (3.11) originates from the region where the conformal weights [8] $n_1 = \pm 1$ and $n_2 = \pm 1$ (see Eq. (2.13)). However it was proven in ref. [8] that BFKL Pomeron states with odd n_1 or n_2 cannot couple to BFKL states where n is even, and therefore this particular divergence does not arise.

The complete scattering amplitude for Fig. 9 is given by the sum of the two contributions of Eq. (3.20) and Eq. (3.26), namely;

$$A_{(1)}(\Delta, \delta y_H | \text{Fig. 9}) = A_{(1)}^{\text{I}}(\Delta, \delta y_H | \text{Fig. 9}) + A_{(1)}^{\text{II}}(\Delta, \delta y_H | \text{Fig. 9}) \quad (3.27)$$

$$\begin{aligned}
&= 2.28 \times 10^{-10} \text{ GeV}^{-2} & (\alpha_s = 0.12) \\
&2.15 \times 10^{-7} \text{ GeV}^{-2} & (\alpha_s = 0.2) \quad (3.28)
\end{aligned}$$

Comparing the results of Eq. (3.20) and Eq. (3.26), it is clear that for the simple Pomeron loop amplitude of Fig. 9, the dominant contribution stems from region II. From an observation of Eq. (3.26), the simple loop amplitude can be written as

$$A_{(1)}^{\text{II}}(\Delta, \delta y_H | \text{Fig. 9}) = k_{(1)} e^{2\omega(0)\Delta} \quad (3.29)$$

where $k_{(1)}$ contains all the other terms included in the simple loop amplitude. From Eq. (3.29) it is clear that the dominant contribution to the loop amplitude is equivalent to the amplitude of 2 non interacting Pomerons. This can be seen from Fig. 9, where by taking the 2 branches of the loop outside, one observes the exchange of 2 non interacting Pomerons. This was first noted by A.Mueller, who commented that at high rapidities, loop diagrams reduce to the exchange of multiple non interacting Pomerons, with renormalized Pomeron vertices (see ref. [5]).

Comparing the results of Eq. (2.24) and Eq. (3.28), the Pomeron loop of Fig. 9 is potentially very close to the basic diagram of Fig. 7 in amplitude, and suggests that Pomeron loop diagrams potentially suppress the enhanced survival probability $\langle |S_{\text{enh}}^2| \rangle$ considerably. However the contribution of higher order multiple Pomeron loop diagrams needs to be included, before any precise statements can be made about the enhanced survival probability. In the next section, the technique used for deriving the amplitude for diagrams with multiple Pomeron loops, will be explained. A good knowledge of how to calculate these type of diagrams is a necessary tool for estimating the contribution of the full set of enhanced diagrams, to the survival probability.

4. The main idea

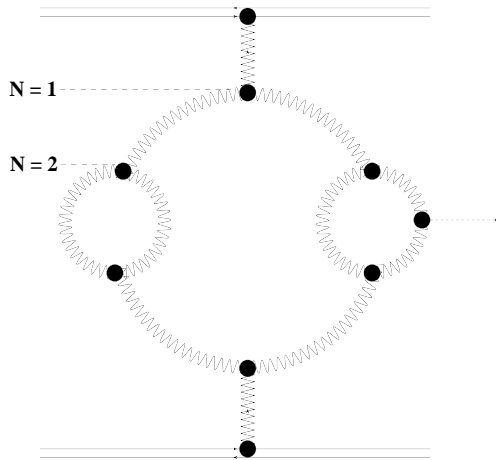


Figure 14: The Pomeron enhanced diagram with $N = 2$ generations of branching.

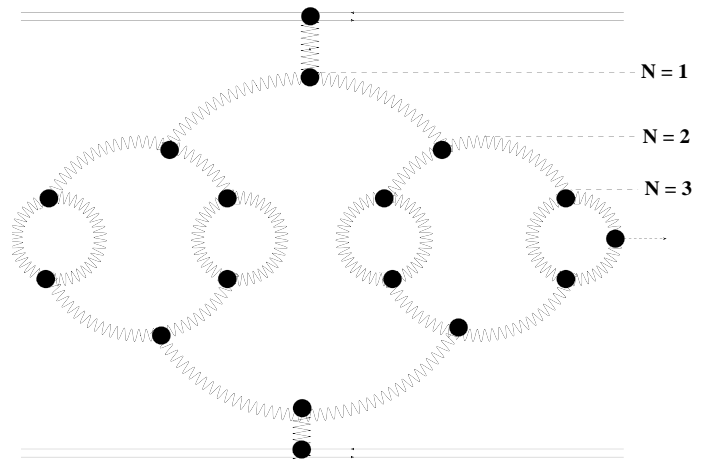


Figure 15: The Pomeron enhanced diagram with $N = 3$ generations of branching.

In this section the approach used to calculate the amplitude of more complicated Pomeron diagrams with more generations of Pomeron branching, such as the diagrams shown in Fig. 14 and Fig. 15, will be explained. Until now the generally accepted technique for estimating the amplitude for Pomeron enhanced diagrams of this type, has been the well known mean field approximation of Mueller-Patel-Salam-Iancu (MPSI). In the previous section, the major contribution to the loop amplitude was shown to be equivalent to 2 non interacting Pomerons. In ref. [7] we showed that the amplitude of any general Pomeron enhanced diagram, is equivalent to the amplitude of the diagram of non interacting Pomerons, with renormalized

Pomeron vertices. This was one of the first steps towards deriving the amplitude of more complicated Pomeron enhanced diagrams, other than the simple loop of Fig. 9 in perturbative QCD. The goal of this section is to show that the amplitude of an arbitrary Pomeron enhanced diagram, can be estimated in the precise QCD approach instead of the MPSI approximation.

To illustrate some examples of Pomeron enhanced diagrams, Fig. 14 shows the enhanced diagram with $N = 2$ generations of branching, and Fig. 15 shows the enhanced diagram with $N = 3$ generations of branching. In Fig. 14, the first generation of splitting forms the larger “embedded” loop, and the second generation of splitting forms the two simple loops at the center of the diagram to form a total of $2^2 - 1 = 3$ loops. Likewise in Fig. 15 there are $2^3 - 1 = 7$ loops. Diagrams such as these can be calculated in perturbative QCD using the following approach. Consider for example Fig. 16 which shows the diagram with N generations of Pomeron branching, leading to a total of $2^N - 1$ loops. In this picture the N generation diagram is equivalent to 2 sets of diagrams with $N - 1$ generations of branching, embedded in one large loop as shown in Fig. 16.

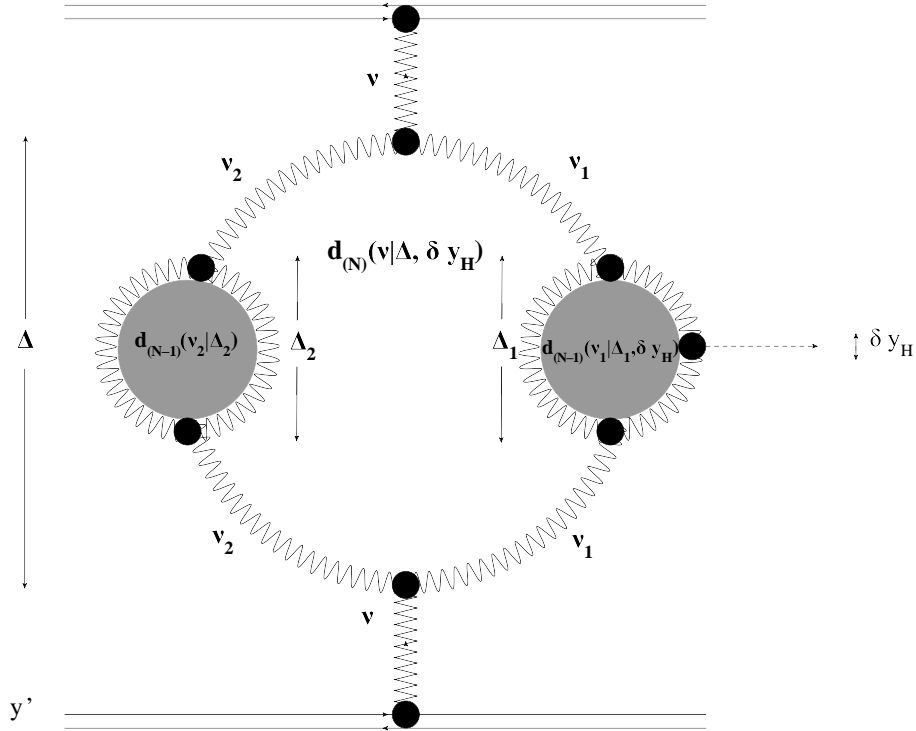


Figure 16: Pictorial representation of the Pomeron enhanced diagram with N generations of branching, as the product of 2 sets of diagrams each with $N - 1$ generations of branching, embedded in one large loop.

From this picture the amplitude $d_{(N)}(\nu|\Delta, \delta y_H)$ of the N generation diagram which occupies a rapidity gap Δ , is a function of the two sets of $N - 1$ generation diagrams embedded in the larger loop, which occupy

a rapidity gap Δ_1 and Δ_2 respectively, so that one can write for the amplitude;

$$d_{(N)}(\nu|\Delta, \delta y_H) = d_{(N-1)}(\nu_1|\Delta_1, \delta y_H) \otimes d_{(N-1)}(\nu_2|\Delta_2) \quad (4.1)$$

where \otimes denotes all necessary integrations over the conformal variables ν_1 and ν_2 , and also over the rapidity gaps Δ_1 and Δ_2 , where $0 \leq \Delta_1 \leq \Delta$, and $\delta y_H \leq \Delta_2 \leq \Delta$. Eq. (4.1) shows the iterative expression which will be used to derive the expression for the arbitrary Pomeron enhanced diagram with N generations of Pomeron branching. The formalism which will be followed is to start from the basic simple loop amplitude $d_{(1)}(\nu|\Delta, \delta y_H)$ derived in section 3, and plug this into the expansion of Eq. (4.1) to yield the amplitude $d_{(2)}(\nu|\Delta, \delta y_H)$ of the $N = 2$ generation diagram shown in Fig. 14. Similarly inserting $d_{(2)}(\nu|\Delta, \delta y_H)$ into Eq. (4.1) gives the amplitude $d_{(3)}(\nu|\Delta, \delta y_H)$ of the $N = 3$ generation diagram shown in Fig. 15. Continuing with this technique, the general expression $d_{(N)}(\nu|\Delta, \delta y_H)$ for the amplitude of the N generation diagram shown in Fig. 17 can be found, using proof by induction.

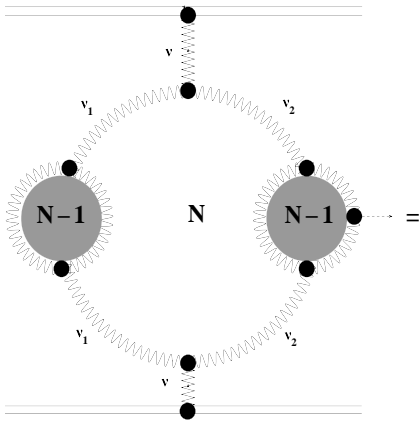


Figure 17: The diagram with N generations of branching, shown as two sets of $N - 1$ generation diagrams embedded in one larger Pomeron loop.

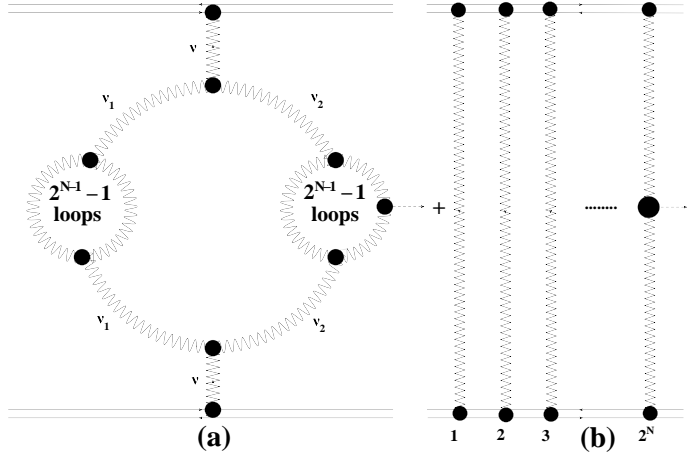


Figure 18: (a) shows the contribution to the N generation diagram amplitude which stems from the region I: $\{\nu, |\nu_1|, |\nu_2|\} = \{0, 1/2, 1/2\}$ and region II: $\{|\nu|, \nu_1, \nu_2\} = \{1/2, 0, 0\}$. Regions I and II lead to the renormalization of the Pomeron intercept, and the loops are preserved. (b) shows the contribution to the amplitude of the N generation diagram, which is equivalent to the amplitude of 2^N non interacting Pomerons, and stems from the region $\{|\nu|, |\nu_1|, |\nu_2|\} = \{1/2, 1/2, 1/2\}$

In section 3 the simple Pomeron loop amplitude was calculated for the two regions I: $\{\nu, |\nu_1|, |\nu_2|\} = \{0, 1/2, 1/2\}$ and II: $\{|\nu|, \nu_1, \nu_2\} = \{1/2, 0, 0\}$. Region I led to the contribution which is the renormalization of the Pomeron intercept (see Eq. (3.19)). Region II led to the contribution to the amplitude which

is equivalent to the amplitude of 2 non interacting Pomerons, with renormalized Pomeron vertices (see Eq. (3.26)). Likewise, calculating the amplitude of the N generation diagram shown in Fig. 17, leads to 2 contributions. The first is the contribution from the renormalization of the Pomeron intercept (see Fig. 18a). The second contribution is from the diagram which is equivalent to 2^N non interacting Pomerons, with renormalized Pomeron vertices, shown in Fig. 18b. These two contributions stem from 3 regions for the conformal variables, where in the notation of Fig. 17, these are region I: $\{\nu, |\nu_1|, |\nu_2|\} = \{0, 1/2, 1/2\}$; region II: $\{|\nu|, \nu_1, \nu_2\} = \{1/2, 0, 0\}$; and region III: $\{|\nu|, |\nu_1|, |\nu_2|\} = \{1/2, 1/2, 1/2\}$. For the diagrams with $N \geq 2$, regions I and II will lead to the contribution shown in Fig. 18a which is equivalent to the renormalization of the Pomeron intercept. For $N \geq 2$ Region III will yield the contribution to the amplitude which is equivalent to 2^N non interacting Pomerons, with renormalized Pomeron vertices. The contributions of all three regions to the amplitude of the N generation diagram can be summarized as;

$$\begin{aligned}
A_{(N)}(\Delta, \delta y_H | \text{Fig. 17}) &= A_{(N)}^{\text{I}}(\Delta, \delta y_H | \text{Fig. 18 a}) + A_{(N)}^{\text{II}}(\Delta, \delta y_H | \text{Fig. 18a}) + A_{(N)}^{\text{III}}(\Delta, \delta y_H | \text{Fig. 18b}) \\
&= k_{(N)}^{\text{I}} e^{\omega(0)\Delta} + k_{(N)}^{\text{II}} e^{2\omega(0)\Delta} + k_{(N)}^{\text{III}} e^{2^N \omega(0)\Delta}
\end{aligned} \tag{4.2}$$

where $k_{(N)}$ are constants which contain all other terms which are included in the amplitude.

5. Multiple-loop Pomeron enhanced diagrams

In this section, the amplitude for diffractive Higgs production from the Pomeron enhanced diagrams with $N = 2$ and $N = 3$ generations of branching, shown in Fig. 19 and Fig. 20 respectively, are derived using the iterative technique outlined in section 4. The resulting expressions for these diagrams, will provide the tools necessary to form a general expression for the diagram with N generations of Pomeron branching, shown in Fig. 21.

The scattering amplitude of Fig. 19 is given by a straightforward extension of Eq. (3.12), namely;

$$A_{(2)}(\Delta, \delta y_H | \text{Fig. 19}) = \frac{\alpha_s^2}{4} \int_{-\infty}^{\infty} d\nu h(\nu) \lambda^2(\nu) e^{\omega(\nu)\Delta} d_{(2)}(\nu | \Delta, \delta y_H) E_\nu E'_{-\nu} A_H \tag{5.1}$$

where $d_{(2)}(\nu | \Delta, \delta y_H)$ labels the contribution to the scattering amplitude of the $2^2 - 1 = 3$ loops which arise from the $N = 2$ generations of Pomeron branching. The order of the symmetry group of the diagram of Fig. 19 is $S_{(1)}S_{(2)}$, where $S_{(1)} = 16$ is associated with the large outer loop from the same considerations discussed in section 3, and $S_{(2)} = 8$ is associated with permutations of the two internal loops, which lead to identical diagrams.

Following the formalism described in Eq. (4.1), $d_{(2)}(\nu | \Delta, \delta y_H)$ is a function of the two simple Pomeron loop amplitudes $d_{(1)}(\nu_1 | \Delta_1, \delta y_H)$ and $d_{(1)}(\nu_2 | \Delta_1)$ embedded in the large loop as shown in Fig. 19. Here

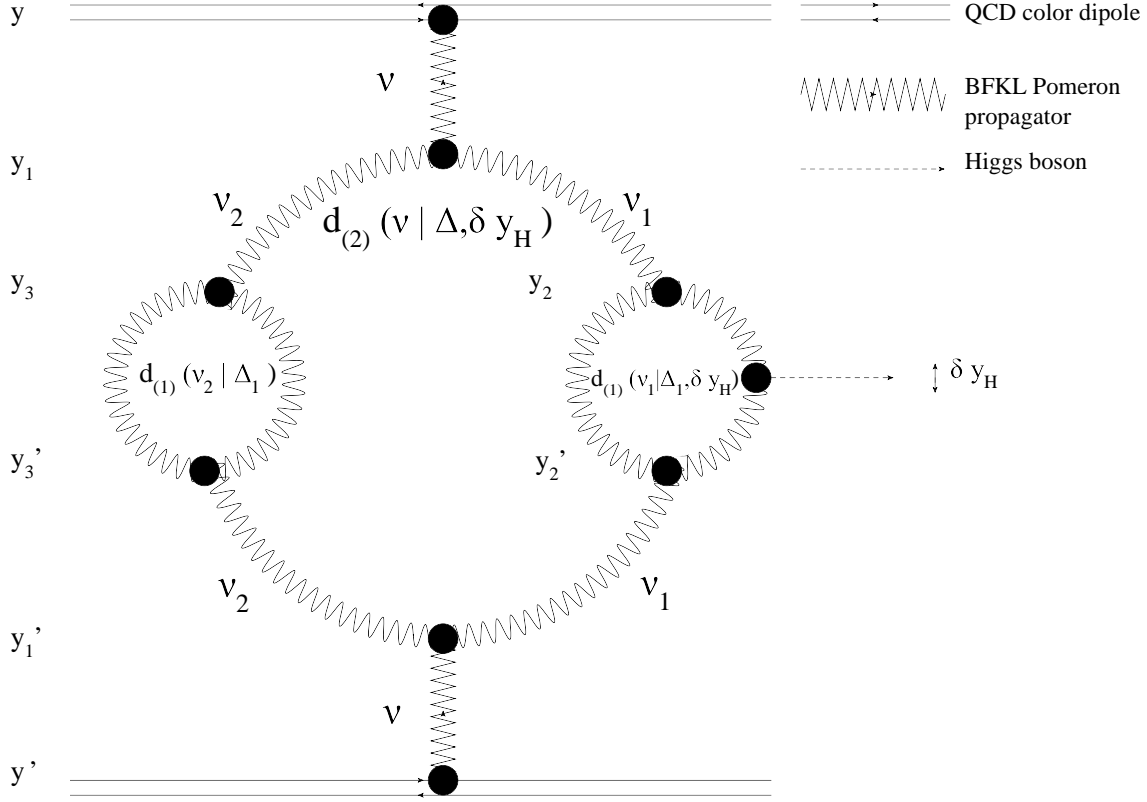


Figure 19: The Pomeron enhanced diagram with $N = 2$ generations of branching, leading to $2^2 - 1 = 3$ loops.

$\Delta_1 = y_1 - y_1'$ is the rapidity gap occupied by the large outer loop in Fig. 19. Hence in this approach, including the symmetry factor $1/S_{(1)}S_{(2)} = 1/2^2$;

$$\begin{aligned}
 d_{(2)}(\nu | \Delta, \delta y_H) &= \frac{1}{2^2} \int_{-\infty}^{\infty} d\nu_1 h(\nu_1) \lambda^2(\nu_1) \int_{-\infty}^{\infty} d\nu_2 h(\nu_2) \lambda^2(\nu_2) \left| \Gamma(\nu | \nu_1, \nu_2) \right|^2 \\
 &\times \int_{y'+\delta y_H}^y dy_1 \int_{y'}^{y_1 - \delta y_H} dy_1' e^{(\omega(\nu_1) + \omega(\nu_2) - \omega(\nu))\Delta_1} d_{(1)}(\nu_1 | \Delta_1, \delta y_H) d_{(1)}(\nu_2 | \Delta_1) \quad (5.2)
 \end{aligned}$$

The simple loop amplitude was derived in Eq. (3.17) and Eq. (3.22) for two different regions. $d_{(1)}(\nu_2 | \Delta_1)$ which labels the internal loop in Fig. 19 to the left without the production of the Higgs boson, is derived from Eq. (3.17) or Eq. (3.22) by setting δy_H equal to zero. By inserting Eq. (3.17) into Eq. (5.2), one can evaluate the integration over the conformal variables for region I: $\{\nu, |\nu_1|, |\nu_2|\} = \{0, 1/2, 1/2\}$ and region II: $\{|\nu|, \nu_1, \nu_2\} = \{1/2, 0, 0\}$. For region I the triple Pomeron vertex derived in Eq. (A.22) should be inserted, and then integrate over ν_1 and ν_2 using the contour C shown in Fig. 13 and sum over the residues at $\{i\nu_1, i\nu_2\} = 1/2$. An extra factor of 2 is included to take into account the identical contribution from

the residues at $\{i\nu_1, i\nu_2\} = -1/2$. Overall after integrating over the rapidity variables, the contribution of region I to Eq. (5.2) is given by the expression;

$$d_{(2)}^{\text{I}}(\nu|\Delta, \delta y_H) = d' d^2 \left(\frac{1}{2} + i\nu\right)^3 \left(\frac{1}{2} - i\nu\right)^3 \chi(\nu) e^{-\omega(\nu)\delta y_H} \\ \times \left\{ \left(6 - \frac{3}{4}\bar{\alpha}_s \delta y_H\right) \omega(\nu) \left(\omega(\nu) + \frac{\omega^2(\nu)(\Delta - \delta y_H)}{3}\right) \right\} \quad (5.3)$$

$$\text{where } d' = \frac{\bar{\alpha}_s^2}{2^{11}} \left(1 - \frac{1}{N_c^2}\right) \left(1 - \frac{2}{N_c^2}\right) \quad (5.4)$$

Inserting Eq. (5.3) into Eq. (5.1) and integrating over ν using the method of steepest descents in the same way described in section 2, yields the following contribution of region I to the scattering amplitude for Fig. 19;

$$A_{(2)}^{\text{I}}(\Delta, \delta y_H | \text{Fig. 19}) = \frac{(2\pi)^{1/2} \bar{\alpha}_s^2 A_H}{128\pi^2 N_c^2} d' d^2 \frac{e^{\omega(0)(\Delta - \delta y_H)}}{(\omega''(0)(\Delta - \delta y_H))^{3/2}} \\ \times \chi(0) \left\{ \left(6 - \frac{3}{4}\bar{\alpha}_s \delta y_H\right) \omega(0) \left(\omega(0) + \frac{\omega^2(0)(\Delta - \delta y_H)}{3}\right) \right\} \quad (5.5)$$

$$= 8.91 \times 10^{-17} \text{ GeV}^{-2} \quad (\alpha_s = 0.12) \\ 3.3 \times 10^{-14} \text{ GeV}^{-2} \quad (\alpha_s = 0.2) \quad (5.6)$$

Alternatively, after inserting Eq. (3.17) into Eq. (5.2), the contribution from region II, namely $\{|\nu|, \nu_1, \nu_2\} = \{1/2, 0, 0\}$ is found by substituting for the triple Pomeron vertex Eq. (A.23) and integrating over the conformal variables ν_1 and ν_2 using the steepest descents method, which yields the expression;

$$d_{(2)}^{\text{II}}(\nu|\Delta, \delta y_H) = a' d^2 \frac{e^{-\omega(0)\delta y_H}}{(1/2 + i\nu)(1/2 - i\nu)} \int_{y'+\delta y_H}^y dy_1 \int_{y'}^{y_1 - \delta y_H} dy'_1 \frac{e^{(2\omega(0) - \omega(\nu))\Delta_1}}{(\Delta_1(\Delta_1 - \delta y_H))^{3/2}} \\ \times \chi^2(0) \left\{ \omega(0) + \frac{1}{2}\omega^2(0)(\Delta_1 - \delta y_H) \right\} \left\{ \omega(0) + \frac{1}{2}\omega^2(0)\Delta_1 \right\} \quad (5.7)$$

$$\text{where } a' = \frac{\bar{\alpha}_s^4}{2^6 \pi N_c^4 [\omega''(0)]^3} \quad (5.8)$$

Inserting Eq. (5.7) into Eq. (5.1) and using the contour C shown in Fig. 13 for the ν integral, the solution is the sum over residues at $i\nu = 1/2$. In the same way an additional factor of 2 includes the

identical contribution from the sum over residues at $i\nu = -1/2$. Using this approach, the contribution of region II to the scattering amplitude of Fig. 19 is;

$$\begin{aligned}
A_{(2)}^{\text{II}}(\Delta, \delta y_H | \text{Fig. 19}) &= \frac{\bar{\alpha}_s a' d^2 A_H}{2^9 \pi N_c^2} \chi^2(0) (\Delta - \delta y_H) \\
&\times \left(\frac{-1}{\bar{\alpha}_s} \frac{d}{d\Delta} \right)^3 \left\{ \frac{e^{2\omega(0)(\Delta - \delta y_H/2)}}{(\Delta(\Delta - \delta y_H))^{3/2}} \left(\omega(0) + \frac{1}{2} \omega^2(0)(\Delta - \delta y_H) \right) \left(\omega(0) + \frac{1}{2} \omega^2(0)\Delta \right) \right\} \quad (5.9) \\
&= 4.94 \times 10^{-17} \text{ GeV}^{-2} \quad (\alpha_s = 0.12) \\
&3.23 \times 10^{-13} \text{ GeV}^{-2} \quad (\alpha_s = 0.2) \quad (5.10)
\end{aligned}$$

Eq. (5.5) and Eq. (5.9) are the contributions to the scattering amplitude of Fig. 19, which lead to the renormalization of the Pomeron intercept. Alternatively, the contribution to Fig. 19 which is equivalent to 4 non interacting Pomerons, is found by substituting for $d_{(1)}(\nu_1 | \Delta_1, \delta y_H)$ and $d_{(1)}(\nu_2 | \Delta_1)$ the simple loop amplitude of Eq. (3.22) in Eq. (5.2), and evaluating the integrals over the conformal variables, taking into account the singularities which arise from region III: $\{|\nu|, |\nu_1|, |\nu_2|\} = \{1/2, 1/2, 1/2\}$. Inserting the triple Pomeron vertex of Eq. (A.22) into Eq. (5.2), the ν_1 and ν_2 integrations are evaluated by summing over the identical residues at $\{i\nu_1, i\nu_2\} = 1/2$ and $-1/2$, which arise from integrating along the contours C and C' shown in Fig. 13, yielding the result;

$$\begin{aligned}
d_{(2)}^{\text{III}}(\nu | \Delta, \delta y_H) &= a^2 b e^{-\omega(0)\delta y_H} (1/2 + i\nu)^3 (1/2 - i\nu)^3 \chi(\nu) \int_{y'+\delta y_H}^y dy_1 \int_{y'}^{y_1 - \delta y_H} dy_1' e^{-\omega(\nu)\Delta_1} \\
&\times (\Delta_1 - \delta y_H) \Delta_1 \left\{ \left(\frac{-1}{\bar{\alpha}_s} \frac{d}{d\Delta_1} \right)^3 \frac{e^{2\omega(0)\Delta_1}}{\Delta_1^{3/2} (\Delta_1 - \delta y_H)^{3/2}} \right\} \left\{ \left(\frac{-1}{\bar{\alpha}_s} \frac{d}{d\Delta_1} \right)^3 \frac{e^{2\omega(0)\Delta_1}}{\Delta_1^3} \right\} \quad (5.11)
\end{aligned}$$

$$\text{where } b = \frac{\bar{\alpha}_s^2}{2^{10}} \left(1 - \frac{1}{N_c^2} \right)^2 \quad (5.12)$$

Inserting Eq. (5.11) into Eq. (5.1), the ν integration is solved using the same method of residues described above, so that the contribution of region III to the scattering amplitude of Fig. 19, which is equivalent to the amplitude of non interacting Pomerons is;

$$\begin{aligned}
A_{(2)}^{\text{III}}(\Delta, \delta y_H | \text{Fig. 19}) &= \frac{\bar{\alpha}_s A_H}{2^9 N_c^2 \pi} a^2 b e^{-\omega(0)\delta y_H} \\
&\times (\Delta - \delta y_H)^2 \Delta \left\{ \left(\frac{-1}{\bar{\alpha}_s} \frac{d}{d\Delta} \right)^3 \frac{e^{2\omega(0)\Delta}}{\Delta^{3/2} (\Delta - \delta y_H)^{3/2}} \right\} \left\{ \left(\frac{-1}{\bar{\alpha}_s} \frac{d}{d\Delta} \right)^3 \frac{e^{2\omega(0)\Delta}}{\Delta^3} \right\} \quad (5.13)
\end{aligned}$$

$$\begin{aligned}
&= 2.85 \times 10^{-15} \text{ GeV}^{-2} \quad (\alpha_s = 0.12) \\
&1.39 \times 10^{-7} \text{ GeV}^{-2} \quad (\alpha_s = 0.2) \quad (5.14)
\end{aligned}$$

From an observation of Eq. (5.13);

$$A_{(2)}^{\text{III}}(\Delta, \delta y_H | \text{Fig. 19}) = k_{(2)} e^{4\omega(0)\Delta} \quad (5.15)$$

where $k_{(2)}$ contains all the other terms contained in the amplitude. The above results show that the main contribution to the the scattering amplitude of Fig. 19 is just the equivalent of 4 non interacting Pomerons, with renormalized Pomeron vertices. The complete scattering amplitude of the $N = 2$ generation diagram of Fig. 19, is the sum over the contributions of Eq. (5.5), Eq. (5.9) and Eq. (5.13), namely;

$$\begin{aligned} A(\Delta, \delta y_H | \text{Fig. 19}) &= A_{(2)}^{\text{I}}(\Delta, \delta y_H | \text{Fig. 19}) + A_{(2)}^{\text{II}}(\Delta, \delta y_H | \text{Fig. 19}) + A_{(2)}^{\text{III}}(\Delta, \delta y_H | \text{Fig. 19}) \quad (5.16) \\ &= 2.85 \times 10^{-15} \text{ GeV}^{-2} \quad (\alpha_s = 0.12) \\ &\quad 1.39 \times 10^{-7} \text{ GeV}^{-2} \quad (\alpha_s = 0.2) \quad (5.17) \end{aligned}$$

Comparing the values of Eq. (3.28) and Eq. (5.17), Fig. 19 is of the same order of magnitude as the simple loop amplitude of Fig. 9. This implies that in order to estimate the enhanced survival probability, it is not enough to just take into account the simple Pomeron loop, but rather also enhanced diagrams with multiple Pomeron loops need to be included in the estimate.

Fig. 20 shows the diagram for diffractive Higgs production in t-channel Pomeron exchange, where there are 3 generations of Pomeron branching, which recombine to form 1 large loop at the $N = 1$ level, 2 smaller internal loops at the $N = 2$ level and 4 simple loops at the $N = 3$ level at the center of the diagram. The scattering amplitude of Fig. 20 is given by the expression;

$$A_{(3)}(\Delta, \delta y_H | \text{Fig. 20}) = \frac{\alpha_s^2}{4} \int_{-\infty}^{\infty} d\nu h(\nu) \lambda^2(\nu) e^{\omega(\nu)\Delta} d_{(3)}(\nu | \Delta, \delta y_H) E_\nu E'_{-\nu} A_H \quad (5.18)$$

where $d_{(3)}(\Delta, \delta y_H)$ is the contribution of the $2^3 - 1 = 7$ loops in Fig. 20 to the scattering amplitude. Following the approach of Eq. (4.1), $d_{(3)}(\Delta, \delta y_H)$ is a function of $d_{(2)}(\Delta_1, \delta y_H)$ and $d_{(2)}(\Delta_1, \delta y_H)$ embedded in the larger outer loop, as shown in Fig. 20. The $N = 3$ generation amplitude $d_{(3)}(\Delta, \delta y_H)$ should also have in the denominator the same symmetry factor $1/2^7$ as for the case of the $N = 2$ generation amplitude, for the same above explained reasons. As such $d_{(3)}(\Delta, \delta y_H)$ is given by the expression;

$$\begin{aligned} d_{(3)}(\nu | \Delta, \delta y_H) &= \frac{1}{2^7} \int_{-\infty}^{\infty} d\nu_1 h(\nu_1) \lambda^2(\nu_1) \int_{-\infty}^{\infty} d\nu_2 h(\nu_2) \lambda^2(\nu_2) \left| \Gamma(\nu | \nu_1, \nu_2) \right|^2 \\ &\quad \times \int_{y'+\delta y_H}^y dy_1 \int_{y'}^{y_1-\delta y_H} dy_1' e^{(\omega(\nu_1)+\omega(\nu_2)-\omega(\nu))\Delta_1} d_{(2)}(\nu_1 | \Delta_1, \delta y_H) d_{(2)}(\nu_2 | \Delta_1) \quad (5.19) \end{aligned}$$

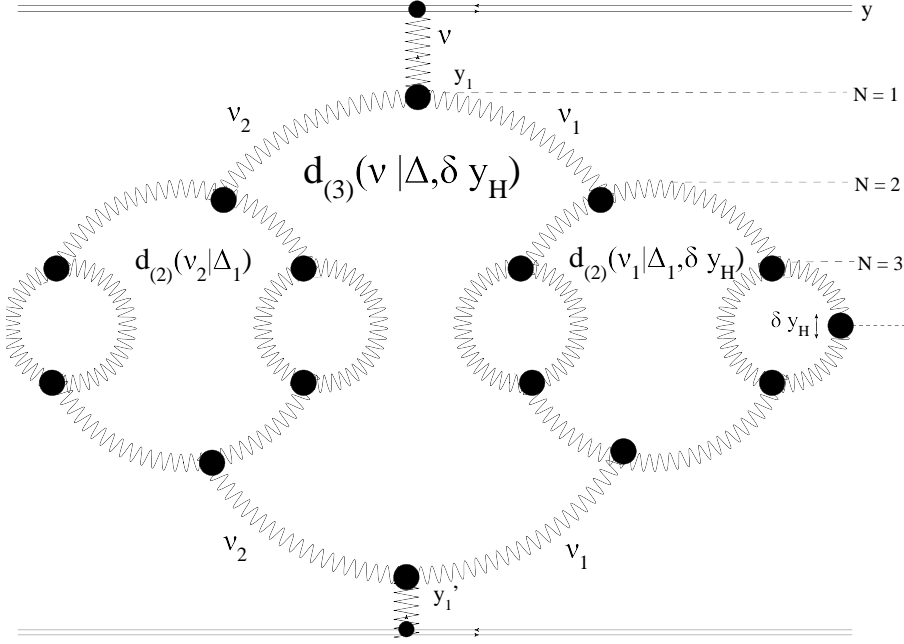


Figure 20: The $N=3$ generation Pomeron loop diagram, leading to $2^3 - 1 = 7$ loops.

Following the same steps as Eq. (5.2) - Eq. (5.13), the contributions of region I and II to Fig. 20 which leads to the renormalization of the Pomeron intercept, and the contribution of region III which is equivalent to the amplitude of non interacting Pomerons are given by the expressions;

$$\begin{aligned}
 A_{(3)}^I(\Delta, \delta y_H | \text{Fig. 20}) &= \frac{(2\pi)^{1/2} \bar{\alpha}_s^3 d^4 d'^3 A_H}{128\pi^2 N_c^2} \frac{e^{\omega(0)(\Delta - \delta y_H)}}{(\omega''(0)(\Delta - \delta y_H))^{3/2}} \chi(0) \\
 &\times 6 \left(6 - \frac{3}{2} \bar{\alpha}_s \delta y_H\right) \left\{ \left(\frac{16}{3} - \frac{4}{9} (2\bar{\alpha}_s) \delta y_H \right) \omega^2(0) \left(\omega(0) + \frac{\omega^2(0)(\Delta - \delta y_H)}{4} \right) \right\} \quad (5.20)
 \end{aligned}$$

$$\begin{aligned}
 &= 3.93 \times 10^{-22} \text{ GeV}^{-2} \quad (\alpha_s = 0.12) \\
 &= 6.27 \times 10^{-18} \text{ GeV}^{-2} \quad (\alpha_s = 0.2) \quad (5.21)
 \end{aligned}$$

$$A_{(3)}^{\text{II}}(\Delta, \delta y_H | \text{Fig. 20}) = \frac{\bar{\alpha}_s a' d^4 d'^2 A_H}{2^9 \pi N_c^2} 6 \left(6 - \frac{3}{4} \bar{\alpha}_s \delta y_H \right) \chi^2(0) \omega^2(0) (\Delta - \delta y_H) \\ \times \left(\frac{-1}{\bar{\alpha}_s} \frac{d}{d\Delta} \right)^3 \left\{ \frac{e^{2\omega(0)(\Delta - \delta y_H/2)}}{(\Delta(\Delta - \delta y_H))^{3/2}} \left(\omega(0) + \frac{\omega^2(0)(\Delta_1 - \delta y_H)}{3} \right) \left(\omega(0) + \frac{\omega^2(0)(\Delta_1 - \delta y_H)}{3} \right) \right\} \quad (5.22)$$

$$= 2.52 \times 10^{-26} \text{ GeV}^{-2} \quad (\alpha_s = 0.12) \\ 8.53 \times 10^{-21} \text{ GeV}^{-2} \quad (\alpha_s = 0.2) \quad (5.23)$$

$$A_{(3)}^{\text{III}}(\Delta, \delta y_H | \text{Fig. 20}) = \frac{\bar{\alpha}_s A_H}{2^9 N_c^2 \pi} a^4 b^3 e^{-\omega(0)\delta y_H} \\ \times \Delta^4 (\Delta - \delta y_H)^3 \left\{ \left(\frac{-1}{\bar{\alpha}_s} \frac{d}{d\Delta} \right)^3 \frac{e^{2\omega(0)\Delta}}{\Delta^{3/2} (\Delta - \delta y_H)^{3/2}} \right\} \left\{ \left(\frac{-1}{\bar{\alpha}_s} \frac{d}{d\Delta} \right)^3 \frac{e^{2\omega(0)\Delta}}{\Delta^3} \right\}^3 \quad (5.24)$$

$$= 3.34 \times 10^{-24} \text{ GeV}^{-2} \quad (\alpha_s = 0.12) \\ 1.28 \times 10^{-7} \text{ GeV}^{-2} \quad (\alpha_s = 0.2) \quad (5.25)$$

Eq. (5.24) is the contribution which is equivalent to the amplitude of 8 non interacting Pomerons, as can be seen clearly by recasting Eq. (5.24) in the following form;

$$A_{(3)}^{\text{III}}(\Delta, \delta y_H | \text{Fig. 20}) = k_{(3)} e^{8\omega(0)\Delta} \quad (5.26)$$

where $k_{(3)}$ contains all other terms included in the amplitude. The major contribution comes from the non interacting Pomeron contribution of Eq. (5.25). The full scattering amplitude of Fig. 20 is the sum over the contributions of Eq. (5.20), Eq. (5.22) and Eq. (5.24), namely;

$$A(\Delta, \delta y_H | \text{Fig. 20}) = A_{(3)}^{\text{I}}(\Delta, \delta y_H | \text{Fig. 20}) + A_{(3)}^{\text{II}}(\Delta, \delta y_H | \text{Fig. 20}) + A_{(3)}^{\text{III}}(\Delta, \delta y_H | \text{Fig. 20}) \quad (5.27)$$

$$= 3.34 \times 10^{-24} \text{ GeV}^{-2} \quad (\alpha_s = 0.12) \\ 1.28 \times 10^{-7} \text{ GeV}^{-2} \quad (\alpha_s = 0.2) \quad (5.28)$$

The value in Eq. (5.28) is very close to the amplitude of Fig. 19 for $\alpha_s = 0.2$ (see Eq. (5.17)) and the same order of magnitude as the amplitude of the simple Pomeron loop of Fig. 9 (see Eq. (3.28)). This shows that in order to obtain an accurate estimate of the enhanced survival probability $\langle |S_{\text{enh}}^2| \rangle$, the sum over the complete set of Pomeron loops needs to be found. This is the subject matter of the next section.

6. The summation over Pomeron loop diagrams

In this section the diffractive Higgs production amplitude from the general multiple Pomeron loop diagram, with N generations of branching is derived. This general expression provides the basis for summing over the complete set of Pomeron loop diagrams, in perturbative QCD, instead of using the MPSI approach. In a diagram with N generations of Pomeron branching shown in Fig. 21, the k^{th} generation of branching gives rise to 2^{k-1} loops, so that in Fig. 21, there are a total of $\sum_{k=1}^N 2^{k-1} = 2^N - 1$ loops. So far 3 contributing regions to the amplitude of Pomeron loops have been discussed. An analytical formula for the diagram with N generations of branching can be derived, for all 3 of these regions using the iterative technique outlined in section 4, without any a priori assumptions. For the diagram of diffractive Higgs production in t-channel Pomeron exchange, where there are N generations of Pomeron branching as shown in Fig. 21, the high energy scattering amplitude is labeled;

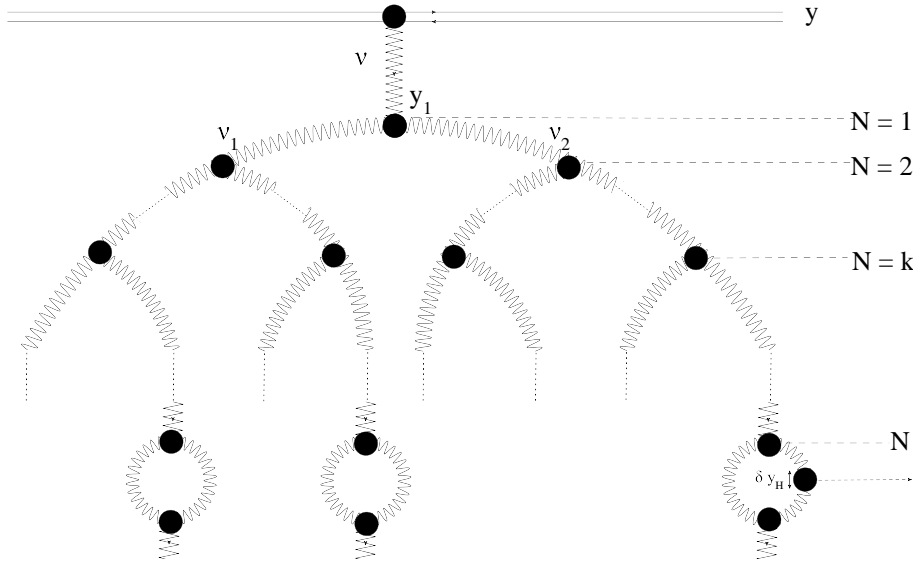


Figure 21: The diagram with N generations of Pomeron branching, leading to $2^N - 1$ loops.

$$A_{(N)}(\Delta, \delta y_H | \text{Fig. 21}) = \frac{\alpha_s^2}{4} \int_{-\infty}^{\infty} d\nu h(\nu) \lambda^2(\nu) e^{\omega(\nu)\Delta} d_{(N)}(\nu | \Delta, \delta y_H) E_\nu E'_{-\nu} A_H \quad (6.1)$$

where the amplitude for the N generations of loops $d_{(N)}(\nu | \Delta, \delta y_H)$ is found from the iterative equation;

$$\begin{aligned}
d_{(N)}(\nu|\Delta, \delta y_H) &= \frac{1}{2^7} \int_{-\infty}^{\infty} d\nu_1 h(\nu_1) \lambda^2(\nu_1) \int_{-\infty}^{\infty} d\nu_2 h(\nu_2) \lambda^2(\nu_2) \left| \Gamma(\nu|\nu_1, \nu_2) \right|^2 e^{-\omega(\nu)\delta y_H} \\
&\times e^{\omega(\nu_2)\delta y_H} \int_{y'+\delta y_H}^y dy_1 \int_{y'}^{y_1-\delta y_H} dy_1' e^{(\omega(\nu_1)+\omega(\nu_2)-\omega(\nu))(\Delta_1-\delta y_H)} \\
&\times d_{(N-1)}(\nu_1|\Delta_1, \delta y_H) d_{(N-1)}(\nu_2|\Delta_1) \quad \forall N \geq 1. \quad (6.2)
\end{aligned}$$

The expression for $d_{(1)}(\nu|\Delta, \delta y_H)$, $d_{(2)}(\nu|\Delta, \delta y_H)$ and $d_{(3)}(\nu|\Delta, \delta y_H)$ for the diagrams of Fig. 9, Fig. 19 and Fig. 20, were derived using the iterative expression of Eq. (6.2). Continuing this process using identical techniques, from observing the outcome expression for $d_{(N)}(\nu|\Delta, \delta y_H)$ for higher values of N , a predictable sequence emerges. From an observation of this sequence, a general formula for $d_{(N)}(\nu|\Delta, \delta y_H)$ can be written for the contribution of region I: ($\{\nu, |\nu_1|, |\nu_2|\} = \{0, 1/2, 1/2\}$), region II: ($\{|\nu|, \nu_1, \nu_2\} = \{1/2, 0, 0\}$) and region III: ($\{|\nu|, |\nu_1|, |\nu_2|\} = \{1/2, 1/2, 1/2\}$). This expression can be proved by induction, whereby provided the formula for $d_{(N)}(\nu|\Delta, \delta y_H)$ is true for $N = 2$, and yields the predicted formula for $N + 1$ by plugging $d_{(N)}(\nu|\Delta, \delta y_H)$ into Eq. (6.2), then the proof is complete. In this formalism the following expressions for the contribution of the above three regions are derived for $d_{(N)}(\nu|\Delta, \delta y_H)$;

$$\begin{aligned}
d_{(N)}^{\text{I}}(\nu|\Delta, \delta y_H) &= \frac{(d d')^{2^{[N-1]}}}{d'} \left(\frac{1}{2} + i\nu \right)^3 \left(\frac{1}{2} - i\nu \right)^3 \chi(\nu) e^{-\omega(\nu)\delta y_H} \\
&\times \prod_{k=2}^N \bar{\alpha}_s^{(k-2)2^{[N-k]}} \left(\frac{k+1}{k} - \frac{(k+3)(k+2)(k+1)}{2k^2} \right)^{2^{[N-k]}-1} \\
&\times \prod_{k=2}^N \left(\frac{k+1}{k} - \frac{(k+3)(k+2)(k+1)}{2k^2} + \frac{k+1}{k^2} \bar{\alpha}_s \delta y_H \right) \\
&\times \omega^{N-1}(\nu) \left(\omega(\nu) + \frac{\omega^2(\nu)(\Delta_1 - \delta y_H)}{N+1} \right) \quad \forall N \geq 1; \quad (6.3)
\end{aligned}$$

$$\begin{aligned}
d_{(N)}^{\text{II}}(\nu|\Delta, \delta y_H) &= \frac{a' d^{2^{[N-1]}} (d')^{2^{[N-2]}}}{(1/2 + i\nu)(1/2 - i\nu)} f(N-1, \delta y_H) f(N-1) e^{-\omega(0)\delta y_H} \\
&\times \int_{y'+\delta y_H}^y dy_1 \int_{y'}^{y_1-\delta y_H} dy_1' \frac{e^{(2\omega(0)-\omega(\nu))\Delta_1}}{(\Delta_1(\Delta_1 - y_H))^{3/2}} \\
&\times \chi^2(0) \omega^{2N-4}(0) \left(\omega(0) + \frac{\omega^2(0)(\Delta_1 - \delta y_H)}{N} \right) \left(\omega(0) + \frac{\omega^2(0)\Delta_1}{N} \right) \quad \forall N \geq 2; \quad (6.4)
\end{aligned}$$

where the function $f(N, \delta y_H)$ is defined by;

$$\begin{aligned}
f(N, \delta y_H) &= \prod_{k=2}^N \bar{\alpha}_s^{(k-2)2^{[N-k]}} \left(\frac{k+1}{k} - \frac{(k+3)(k+2)(k+1)}{2k^2} \right)^{2^{[N-k]-1}} \\
&\times \prod_{k=2}^N \left(\frac{k+1}{k} - \frac{(k+3)(k+2)(k+1)}{2k^2} + \frac{k+1}{k^2} \bar{\alpha}_s \delta y_H \right); \tag{6.5}
\end{aligned}$$

and $f(N-1) = f(N-1, \delta y_H = 0)$ can be read off Eq. (6.5) by setting $\delta y_H = 0$, and

$$\begin{aligned}
d_{(N)}^{\text{III}}(\nu|\Delta, \delta y_H) &= \frac{(ab)^{2^{[N-1]}}}{b} e^{-\omega(0)\delta y_H} \int_{y'+\delta y_H}^y dy_1 \int_{y'}^{y_1-\delta y_H} dy'_1 \Delta_1^{2^N-N-1} (\Delta_1 - \delta y_H)^{N-1} e^{-\omega(\nu)\Delta_1} \\
&\times \left\{ \left(\frac{-1}{\bar{\alpha}_s} \frac{d}{d\Delta_1} \right)^3 \frac{e^{2\omega(0)\Delta_1}}{\Delta_1^{3/2} (\Delta_1 - \delta y_H)^{3/2}} \right\} \left\{ \left(\frac{-1}{\bar{\alpha}_s} \frac{d}{d\Delta_1} \right)^3 \frac{e^{2\omega(0)\Delta_1}}{\Delta_1^3} \right\}^{2^{[N-1]-1}} \quad \forall N \geq 2. \tag{6.6}
\end{aligned}$$

where the full set of constants are;

$$\begin{aligned}
d &= \bar{\alpha}_s \left(1 - \frac{1}{N_c^2} \right) \left(1 - \frac{2}{N_c^2} \right); & d' &= \frac{\bar{\alpha}_s^2}{2^{11}} \left(1 - \frac{1}{N_c^2} \right) \left(1 - \frac{2}{N_c^2} \right); \\
a &= \frac{2^9 \bar{\alpha}_s^4}{N_c^4 \pi [\omega''(0)]^3}; & a' &= \frac{\bar{\alpha}_s^4}{2^6 N_c^4 \pi [\omega''(0)]^3}; & b &= \frac{\bar{\alpha}_s^2}{2^{10}} \left(1 - \frac{1}{N_c^2} \right)^2. \tag{6.7}
\end{aligned}$$

Inserting the formulae of Eq. (6.3), Eq. (6.4) and Eq. (6.6) into Eq. (6.1), one finds the following expressions for the contributions of regions I, II and III to the scattering amplitude for diffractive Higgs production, from the N generation diagram of Fig. 21;

$$\begin{aligned}
A_{(N)}^{\text{I}}(\Delta, \delta y_H | \text{Fig. 21}) &= \frac{(2\pi)^{1/2} \bar{\alpha}_s^2 A_H}{128\pi^2 N_c^2} \frac{(d d')^{2^{[N-1]}}}{d'} \frac{e^{\omega(0)(\Delta - \delta y_H)}}{(\omega''(0)(\Delta - \delta y_H))^{3/2}} \chi(0) \\
&\times \prod_{k=2}^N \bar{\alpha}_s^{(k-2)2^{[N-k]}} \left(\frac{k+1}{k} - \frac{(k+3)(k+2)(k+1)}{2k^2} \right)^{2^{[N-k]}-1} \\
&\times \prod_{k=2}^N \left(\frac{k+1}{k} - \frac{(k+3)(k+2)(k+1)}{2k^2} + \frac{k+1}{k^2} \bar{\alpha}_s \delta y_H \right) \\
&\times \omega^{N-1}(0) \left(\omega(0) + \frac{\omega^2(0)(\Delta - \delta y_H)}{N+1} \right) \quad \forall N \geq 1; \quad (6.8)
\end{aligned}$$

$$\begin{aligned}
A_{(N)}^{\text{II}}(\Delta, \delta y_H | \text{Fig. 21}) &= \frac{\bar{\alpha}_s A_H}{2^9 \pi N_c^2} a' d^{2^{[N-1]}} (d')^{2^{[N-2]}} \\
&\times f(N-1, \delta y_H) f(N-1) \chi^2(0) \omega^{2N-4}(0) (\Delta - \delta y_H) \\
&\times \left(\frac{-1}{\bar{\alpha}_s} \frac{d}{d\Delta} \right)^3 \left\{ \frac{e^{2\omega(0)(\Delta - \delta y_H/2)}}{(\Delta(\Delta - y_H))^{3/2}} \left(\omega(0) + \frac{\omega^2(0)(\Delta - \delta y_H)}{N} \right) \right. \\
&\quad \left. \left(\omega(0) + \frac{\omega^2(0)\Delta}{N} \right) \right\} \quad \forall N \geq 2; \quad (6.9)
\end{aligned}$$

$$\begin{aligned}
A_{(N)}^{\text{III}}(\Delta, \delta y_H | \text{Fig. 21}) &= \frac{\bar{\alpha}_s A_H (ab)^{2^{[N-1]}}}{2^9 N_c^2 \pi b} e^{-\omega(0)\delta y_H} \Delta^{2^N - N - 1} (\Delta - \delta y_H)^N \\
&\times \left\{ \left(\frac{-1}{\bar{\alpha}_s} \frac{d}{d\Delta} \right)^3 \frac{e^{2\omega(0)\Delta}}{\Delta^{3/2} (\Delta - \delta y_H)^{3/2}} \right\} \left\{ \left(\frac{-1}{\bar{\alpha}_s} \frac{d}{d\Delta} \right)^3 \frac{e^{2\omega(0)\Delta}}{\Delta^3} \right\}^{2^{[N-1]}-1} \quad \forall N \geq 2; \quad (6.10)
\end{aligned}$$

Eq. (6.8) and Eq. (6.9) are the contributions to the amplitude of the N generation diagram of Fig. 21 which leads to the renormalization of the Pomeron intercept. Eq. (6.10) is the contribution to Fig. 21 which is equivalent to the amplitude of 2^N non interacting Pomerons, with renormalized Pomeron vertices. This can be seen by observing that Eq. (6.10) can be written in the form;

$$A_{(N)}^{\text{III}}(\Delta, \delta y_H | \text{Fig. 21}) = k_{(N)} e^{2^N \omega(0)\Delta} \quad (6.11)$$

where $k_{(N)}$ includes all other terms contained in the amplitude. The complete expression for the scattering amplitude of Fig. 21 is the sum of the contributions of Eq. (6.8), Eq. (6.9) and Eq. (6.10), namely;

$$\begin{aligned}
A_{(N)}(\Delta, \delta y_H | \text{Fig. 21}) \\
= A_{(N)}^{\text{I}}(\Delta, \delta y_H | \text{Eq. (6.8)}) + A_{(N)}^{\text{II}}(\Delta, \delta y_H | \text{Eq. (6.9)}) + A_{(N)}^{\text{III}}(\Delta, \delta y_H | \text{Eq. (6.10)}) \quad (6.12)
\end{aligned}$$

	$A_{(N)}(\Delta = 19, \delta y_H = \ln(M_H^2/4s_0))$	
	$\alpha_s = 0.12$	$\alpha_s = 0.2$
$N = 0$	1.57×10^{-8}	2.17×10^{-7}
$N = 1$	2.05×10^{-10}	2.15×10^{-7}
$N = 2$	2.85×10^{-15}	1.39×10^{-7}
$N = 3$	3.40×10^{-24}	1.28×10^{-7}
$N = 4$	8.20×10^{-42}	2.31×10^{-8}
$N = 5$	8.13×10^{-77}	5.11×10^{-9}
$N = 6$	1.36×10^{-146}	4.26×10^{-10}

Table 1: Results for the scattering amplitude for diffractive Higgs production from the multi Pomeron loop diagram with N generations of Pomeron branching, for the contribution of regions I , II and III. The mass of the Higgs boson is assumed to be $M_H = 100$ GeV, and the rapidity gap Δ between the scattering protons is taken to be $\Delta = 19$, based on proton proton collisions at the typical LHC energy $\sqrt{s} = 14$ TeV.

Table 1 lists the results for the multiple Pomeron loop amplitudes for $\alpha_s = 0.12$ and $\alpha_s = 0.2$. The greatest contribution to Pomeron enhanced diagrams stems from region III, which leads to the contribution to the amplitude which is equivalent to the amplitude of non interacting Pomerons. The values in the table indicate that the amplitude of the N generation diagram becomes smaller as N grows, for energies within the LHC range. The difference in values for different values of α_s show that the amplitude is very sensitive to the choice of the Pomeron intercept. The sum over Pomeron loop diagrams from $N = 0$ (so that the basic diagram of Fig. 7 is included), takes the following form;

$$\Sigma(\Delta, \delta y_H) = A_{(0)}(\Delta, \delta y_H | \text{Fig. 7; Eq. (2.24)}) + \sum_{N=1}^{\infty} (-1)^N A_{(N)}(\Delta, \delta y_H | \text{Eq. (6.12)}) \quad (6.13)$$

Fig. 22 shows the plot for the amplitude of the single Pomeron diagram derived in Eq. (2.24), for the basic diagram shown in Fig. 7 (upper line), next to the plot for the sum over Pomeron loops $\Sigma(\Delta, \delta y_H | \text{Eq. (6.13)})$ up to $N = 20$ (lower line), against the rapidity separation Δ between the incoming projectiles. From an observation of Fig. 22 it is clear that for rapidity values approaching the typical LHC range $\Delta = 19$, $\Sigma(\Delta, \delta y_H | \text{Eq. (6.13)})$ starts to be substantially less than the basic single Pomeron amplitude, as the two graphs grow further apart. This proves that the shadowing correction of Pomeron loops to the basic diagram of Fig. 7, is large within the LHC range of energies. As the rapidity separation between the scattering protons increases, the effect of this shadowing correction increases.

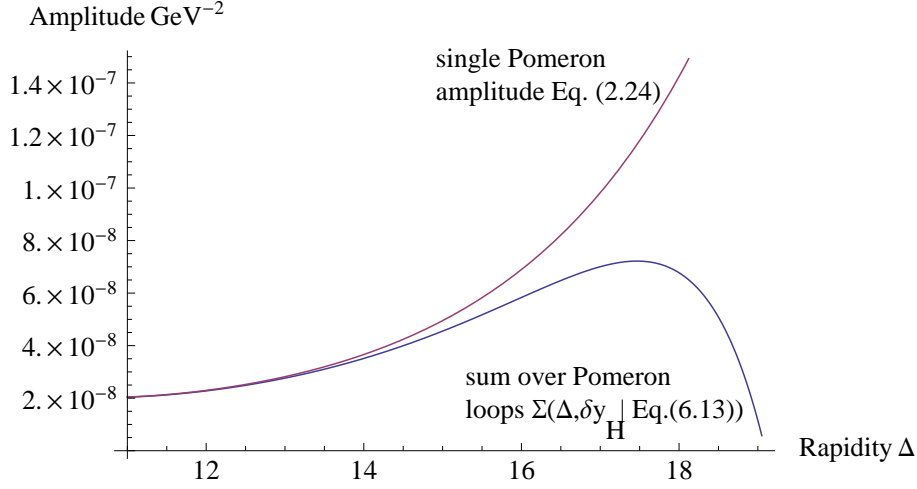


Figure 22: Plot for the single Pomeron amplitude $A_{(0)}(\Delta, \delta y_H | \text{Fig. 7})$ derived in Eq. (2.24) (upper line), next to the plot for the sum over Pomeron loops $\Sigma(\Delta, \delta y_H | \text{Eq. (6.13)})$ up to $N = 20$ (lower line), against the rapidity separation $\Delta = y - y'$ between the scattering protons. The values of Δ go from $\delta y_H = \ln(M_H^2/4s_0)$ (assuming the Higgs mass $M_H = 100 \text{ GeV}$ and $s_0 = 1 \text{ GeV}^2$), up to the typical LHC rapidity $\Delta = 19$. $\alpha_s = 0.2$.

7. The survival probability for exclusive Higgs production

This section is limited to an estimate of the contribution of enhanced diagrams to the survival probability $\langle |S_{\text{enh}}^2| \rangle$ of large rapidity gaps, in exclusive diffractive Higgs production shown in Fig. 7. In section 6 the sum over Pomeron enhanced diagrams in Eq. (6.13) was derived in the exact QCD approach, thanks to the expressions of Eq. (6.8), Eq. (6.9) and Eq. (6.10). This means that the complete set of hard re-scattering contributions to the enhanced survival probability can be estimated in QCD to any order, without relying on the mean field approximation approach.

The enhanced survival probability $\langle |S_{\text{enh}}^2| \rangle$ is estimated by subtracting from the basic diagram of Fig. 7, the first enhanced diagram of Fig. 9, and subtract from this the second enhanced diagram of Fig. 19 and so on. Finally divide by the amplitude of the basic diagram of Fig. 7 to give the correctly normalized survival probability as the expression;

$$\begin{aligned}
& \langle |S_{\text{enh}}^2| \rangle \\
&= \frac{A_{(0)}(\Delta, \delta y_H | \text{Fig. 7}) - A_{(1)}(\Delta, \delta y_H | \text{Fig. 9}) + A_{(2)}(\Delta, \delta y_H | \text{Fig. 19}) - \dots - A_{(N)}(\Delta, \delta y_H | \text{Fig. 20})}{A_{(0)}(\Delta, \delta y_H | \text{Fig. 7})} \\
&= \sum_{N=0}^{\infty} (-1)^N \frac{A_{(N)}(\Delta, \delta y_H)}{A_{(0)}(\Delta, \delta y_H)} \tag{7.1}
\end{aligned}$$

where $A_{(0)}(\Delta, \delta y_H)$ [Fig. 7) was calculated in Eq. (2.24) and all the subsequent terms $A_{(N)}(\Delta, \delta y_H) \quad \forall N \geq 1$ are the sum over Pomeron loops given in Eq. (6.8) - Eq. (6.12)

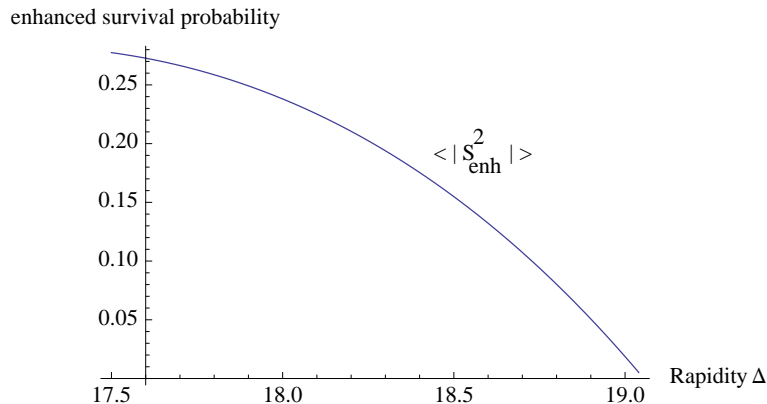


Figure 23: The enhanced survival probability $\langle |S_{\text{enh}}^2| \rangle$ plotted against the rapidity separation Δ of the scattering protons. $\alpha_s = 0.2$.

The results for the enhanced survival probability $\langle |S_{\text{enh}}^2| \rangle$ are shown in the graph of Fig. 23 against the rapidity separation Δ between the incoming projectiles, where all the terms in Eq. (7.1) up to $N = 20$ have been taken into account. The results of Fig. 23 show that $\langle |S_{\text{enh}}^2| \rangle$ is small, and could be even less than 1% for the LHC range of rapidity values, in agreement with refs. [3, 4]. The observation from Fig. 23 that $\langle |S_{\text{enh}}^2| \rangle$ decreases as the rapidity gap Δ between the scattering protons increases, also matches with the findings of refs. [3, 4]. However Fig. 23 shows a steeper rise in $\langle |S_{\text{enh}}^2| \rangle$ as the rapidity separation Δ decreases than the results found in refs. [3, 4], where the improved Mueller-Patel-Salam-Iancu (MPSI) approach was used. We believe this difference in the slope of the graph for $\langle |S_{\text{enh}}^2| \rangle$, shows that there are more complicated diagrams to take into account other than those diagrams considered here, which would lead to a result for $\langle |S_{\text{enh}}^2| \rangle$ which shows a more gradual increase as the rapidity gap Δ decreases. This will be discussed in more detail in the conclusion section.

8. Conclusion

The main achievements of this paper are the following;

1. The observation that the major contribution to the Pomeron loop amplitude stems from the non planar piece of the Korchesky triple Pomeron vertex of Fig. 12
2. The derivation of the general analytical expression for the diagram with an arbitrary number of Pomeron loops, found in Eq. (6.8) - Eq. (6.12).
3. The finding that the main contribution to the amplitude of multiple Pomeron loop diagrams, is equivalent to the amplitude of non interacting Pomerons.

4. The solution to the summation over Pomeron loop diagrams, for the first time in the exact QCD approach.
5. Estimation of the contribution of Pomeron enhanced diagrams to the survival probability $\langle |S_{\text{enh}}^2| \rangle$ for diffractive Higgs production in the QCD formalism, instead of the MFA approach.

The main achievements of this paper are the formulae of Eq. (6.8) - Eq. (6.12) for the amplitude of the multiple Pomeron loop diagram, with N generations of Pomeron branching as shown Fig. 21. It was found that there are 3 regions which contribute to Pomeron loop diagrams. Regions I and II lead to the renormalization of the Pomeron intercept. Region III leads to the contribution to Pomeron loop diagrams, which is equivalent to the amplitude of non interacting Pomerons, with renormalized Pomeron vertices. The contribution from non interacting Pomerons, gives the greatest contribution to the amplitude of Pomeron loop diagrams. The property of the equivalence of Pomeron loop diagrams to non interacting Pomerons, was first noticed by A. Mueller (see ref. [5]). We showed in ref. [7], that if the sum over Pomeron loops was performed in the QCD approach, then the summation should reduce to the sum over non interacting Pomerons diagrams. Therefore the findings in this paper are in agreement with the results in the above mentioned papers.

The sum over Pomeron loop diagrams yields a significant shadowing correction to the basic single Pomeron diagram of Fig. 7. The shadowing correction however is only significant for a rapidity separation between the incoming protons $\Delta \geq 14$, and the shadowing correction becomes larger as the rapidity separation grows (see Fig. 22). We did not take into account the diagrams which contribute to the vertex in the framework of the Schwinger-Dyson equation. However, since the intercept of the Pomeron $\Delta > 0$ as was shown in refs. [5, 7], these diagrams give a small contribution.

The application of the sum over Pomeron enhanced diagrams to an estimate of the enhanced survival probability $\langle |S_{\text{enh}}^2| \rangle$, produced a result which shows that $\langle |S_{\text{enh}}^2| \rangle$ is potentially less than 1% for a typical LHC rapidity separation $\Delta = 19$. From an observation of Fig. 23, $\langle |S_{\text{enh}}^2| \rangle$ decreases as the rapidity separation Δ increases (see Fig. 23). Both of these findings are in agreement with refs. [3, 4]. This comparison shows that the summation over Pomeron enhanced diagrams in the formalism of this paper, reproduces the expected behavior of $\langle |S_{\text{enh}}^2| \rangle$ with rapidity separation Δ . The estimates for the LHC range of rapidity values are close to the previous estimates of refs. [3, 4] (i.e. less than 1%).

The behavior of the enhanced survival probability as a function of the rapidity separation, is a property which stems from the definition of the survival probability. That is the survival probability is a quantitative measure of the effect of shadowing corrections, that stem from inelastic scattering emerging from extra parton showers in the reaction proton + proton \rightarrow proton + [LRG] + Higgs + [LRG] + proton, (where [LRG] denotes a large rapidity gap). Increasing the energy of this reaction leads to a rise in the number of extra parton showers, which spoil the large rapidity gaps as shown in Fig. 3. This leads to the natural conclusion that as the rapidity separation between the scattering protons increases, the survival probability

decreases as more unwanted parton showers arise.

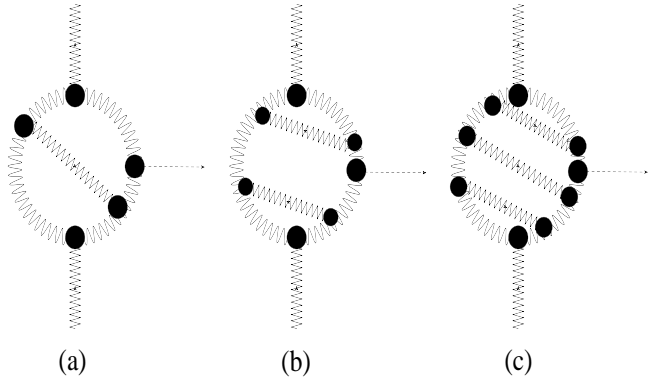


Figure 24: More complicated Pomeron enhanced diagrams that have not yet been taken into account. (a) shows a diagram with $N = 2$ generations of Pomeron branching, (b) shows $N = 3$ and (c) shows $N = 4$ generations of branching.

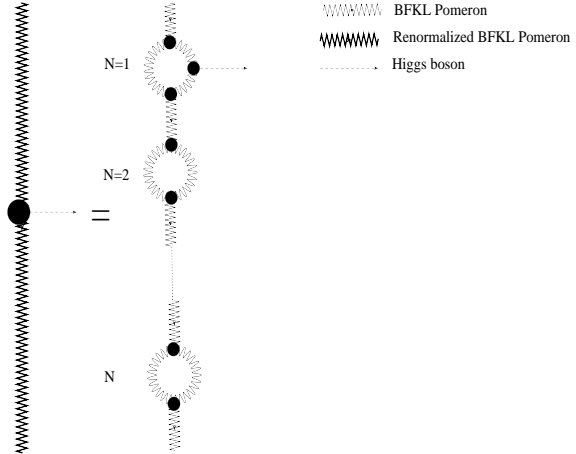


Figure 25: Schematic representation of loop corrections that leads to the renormalized BFKL Pomeron propagator.

The slope of $\langle |S_{\text{enh}}^2| \rangle$ of Fig. 23 with the rapidity separation is steeper than the findings of refs. [3, 4], which relied on an improved (MPSI) model. This observation we believe shows that the summation over Pomeron loops in this paper, while this is an important step forward, is possibly not yet complete.

For example, more complicated enhanced diagrams such as those shown in Fig. 24 could provide an important contribution to the enhanced survival probability, which would lead to a behavior with a less steep increase with rapidity separation. The diagrams in Fig. 24 are not topologically equivalent to any of the other enhanced diagrams discussed in this paper. Since multiple Pomeron loop diagrams decrease with the number of generations of branching N , diagrams (a), (b) and (c) in Fig. 24 which belong to the $N = 2$, $N = 3$ and $N = 4$ class of loop diagrams are not expected to be larger than the simple Pomeron loop diagram of Fig. 9, however their contribution to the summation over enhanced diagrams could affect the slope of Fig. 23 to make it less steep. There is also the issue of the renormalization of the BFKL Pomeron which needs to be taken into account. For example diagrams such as Fig. 25, which although are not expected to be large for any value of N could still provide an important contribution to $\langle |S_{\text{enh}}^2| \rangle$, which would make the slope with rapidity separation not as steep.

We hope that the findings of this paper will be useful for experiments aimed at discovering the Higgs boson at the LHC. We also hope that the methods developed in this paper will provide an important foundation for future calculations of BFKL Pomeron loop diagrams.

9. Acknowledgements

This paper is dedicated to my Grandmother. I would like to thank E. Levin for helpful advice in writing this paper. I would also like to thank L. Apolinário, M. Braun, J. Dias De Deus, and A. Vale for fruitful discussions on the subject. I would also like to thank my wife, Sharon. This research was supported by the Fundação para ciência e a tecnologia (FCT), and CENTRA - Instituto Superior Técnico (IST), Lisbon.

A. The triple Pomeron vertex

In this section of the appendix the derivation of the triple Pomeron vertex, which was first done by Korchemsky in ref. [1] will be outlined. The triple Pomeron vertex is the vertex of three BFKL Pomeron states, which couple either as shown in the planar diagram of Fig. 11, or they couple in the way shown in the non planar diagram of Fig. 12. The coupling of three BFKL Pomeron states with the center of mass coordinates R , R_1 and R_2 and the conformal weights γ , γ_1 and γ_2 is given by for the planar and non-planar diagrams respectively;

$$\Omega(\nu | \nu_1, \nu_2 | \text{Fig. 11}) = \int d^2 R \int d^2 R_1 \int d^2 R_2 \frac{1}{|R_{01}|^2 |R_{12}|^2 |R_{20}|^2} E_\gamma E_{\gamma_1} E_{\gamma_2} \quad (\text{A.1})$$

$$\Lambda(\nu | \nu_1, \nu_2 | \text{Fig. 12}) = \int d^2 R_0 \int d^2 R_1 \frac{1}{|R_{01}|^4} E_\gamma E_{\gamma_1} E_{\gamma_2} \quad (\text{A.2})$$

The leading contribution to the high energy scattering amplitude stems from the region where all the conformal spins vanish, namely $n = n_1 = n_2 = 0$. Adding together Eq. (A.1) and Eq. (A.2) and integrating over the complex coordinates, the triple Pomeron vertex takes the form;

$$\Gamma(\nu | \nu_1, \nu_2) = \left(\frac{\alpha_s N_c}{\pi} \right)^2 \{4\nu^2 + 1\}^2 \left(\Omega(\nu | \nu_1, \nu_2) + \frac{2\pi}{N_c^2} \Lambda(\nu | \nu_1, \nu_2) \{ \chi(\nu) - \chi(\nu_1) - \chi(\nu_2) \} \right) \quad (\text{A.3})$$

where $\chi(\nu)$ is the function;

$$\chi(\nu) = \Re e \left\{ \psi(1) - \psi \left(\frac{1}{2} + i\nu \right) \right\} \quad (\text{A.4})$$

and where

$$\begin{aligned} \Omega(\nu | \nu_1, \nu_2) &= \pi^3 \left\{ \Gamma^2 \left(\frac{1}{2} + i\nu \right) \Gamma^2 \left(\frac{1}{2} + i\nu_1 \right) \Gamma \left(\frac{1}{2} - i\nu \right) \Gamma \left(\frac{1}{2} - i\nu_1 \right) \Gamma \left(\frac{1}{2} - i\nu_2 \right) \right\}^{-1} \\ &\times J^a(\nu, \nu_1, \nu_2) \tilde{J}_a(\nu, \nu_1, \nu_2) \end{aligned} \quad (\text{A.5})$$

where the contracted a index implies summation over $a = 1, 2, 3$. The integrals $J_a(\nu, \nu_1, \nu_2)$ and $\tilde{J}_a(\nu, \nu_1, \nu_2)$ were evaluated in ref. [1], where they were found to be;

$$\begin{aligned}
J_1(\nu, \nu_1, \nu_2) &= \Gamma\left(\frac{1}{2} + i\nu + i\nu_1 - i\nu_2\right) \Gamma\left(\frac{1}{2} + i\nu\right) \Gamma\left(\frac{1}{2} - i\nu\right) \Gamma\left(\frac{1}{2} + i\nu_1\right) \Gamma\left(\frac{1}{2} - i\nu_1\right) \\
&\times \int_0^1 dx (1-x)^{-1/2-i\nu_2} {}_2F_1\left(\frac{1}{2} + i\nu, \frac{1}{2} - i\nu; 1|x\right) {}_2F_1\left(\frac{1}{2} + i\nu_1, \frac{1}{2} - i\nu_1; 1|x\right) \\
J_2(\nu, \nu_1, \nu_2) &= \Gamma\left(\frac{1}{2} + i\nu + i\nu_1 - i\nu_2\right) \Gamma\left(\frac{1}{2} + i\nu\right) \Gamma\left(\frac{1}{2} - i\nu\right) \Gamma\left(\frac{1}{2} + i\nu_1\right) \Gamma\left(\frac{1}{2} - i\nu_1\right) \\
&\times \frac{\Gamma^2\left(\frac{1}{2} - i\nu_2\right)}{\Gamma(1 + i\nu - i\nu_2) \Gamma(1 - i\nu - i\nu_2)} \\
&\times {}_4F_3\left(\frac{1}{2} + i\nu_1, \frac{1}{2} - i\nu_1, \frac{1}{2} - i\nu_2, \frac{1}{2} - i\nu_2 \mid 1 + i\nu - i\nu_2, 1 - i\nu - i\nu_2, 1 \mid 1\right) \\
J_3(\nu, \nu_1, \nu_2) &= \Gamma\left(\frac{1}{2} + i\nu + i\nu_1 - i\nu_2\right) \Gamma\left(\frac{1}{2} + i\nu\right) \Gamma\left(\frac{1}{2} - i\nu\right) \Gamma\left(\frac{1}{2} + i\nu_1\right) \Gamma\left(\frac{1}{2} - i\nu_1\right) \\
&\times \frac{\Gamma^2\left(\frac{1}{2} - i\nu_2\right)}{\Gamma(1 + i\nu_1 - i\nu_2) \Gamma(1 - i\nu_1 - i\nu_2)} \\
&\times {}_4F_3\left(\frac{1}{2} + i\nu, \frac{1}{2} - i\nu, \frac{1}{2} - i\nu_2, \frac{1}{2} - i\nu_2 \mid 1 + i\nu_1 - i\nu_2, 1 - i\nu_1 - i\nu_2, 1 \mid 1\right) \\
\tilde{J}_1(\nu, \nu_1, \nu_2) &= \frac{\Gamma\left(\frac{1}{2} + i\nu\right) \Gamma^2\left(\frac{1}{2} - i\nu\right) \Gamma\left(\frac{1}{2} + i\nu_1\right) \Gamma^2\left(\frac{1}{2} - i\nu_1\right)}{\Gamma\left(\frac{1}{2} - i\nu_2\right) \Gamma(1/2 - i\nu - i\nu_1 + i\nu_2)} \\
&\times \int_0^1 dx x^{-1/2-i\nu_2} (1-x)^{-1/2+i\nu_2-i\nu-i\nu_1} {}_2F_1\left(\frac{1}{2} - i\nu, \frac{1}{2} - i\nu; 1|x\right) {}_2F_1\left(\frac{1}{2} - i\nu_1, \frac{1}{2} - i\nu_1; 1|x\right) \\
\tilde{J}_2(\nu, \nu_1, \nu_2) &= \frac{\Gamma\left(\frac{1}{2} + i\nu_1\right) \Gamma\left(\frac{1}{2} + i\nu_2\right) \Gamma\left(\frac{1}{2} - i\nu\right) \Gamma^2\left(\frac{1}{2} - i\nu_1\right)}{\Gamma(1/2 - i\nu - i\nu_1 + i\nu_2)} \\
&\times \int_0^1 (1-x)^{-1/2-i\nu-i\nu_1+i\nu_2} {}_2F_1\left(\frac{1}{2} - i\nu, \frac{1}{2} - i\nu; 1|x\right) {}_2F_1\left(\frac{1}{2} - i\nu_1, \frac{1}{2} - i\nu_1; 1|x\right) \\
\tilde{J}_3(\nu, \nu_1, \nu_2) &= \frac{\Gamma\left(\frac{1}{2} + i\nu\right) \Gamma\left(\frac{1}{2} + i\nu_2\right) \Gamma\left(\frac{1}{2} - i\nu_1\right) \Gamma^2\left(\frac{1}{2} - i\nu\right)}{\Gamma(1/2 - i\nu - i\nu_1 + i\nu_2)} \\
&\times \int_0^1 (1-x)^{-1/2-i\nu-i\nu_1+i\nu_2} {}_2F_1\left(\frac{1}{2} - i\nu, \frac{1}{2} - i\nu; 1|x\right) {}_2F_1\left(\frac{1}{2} - i\nu_1, \frac{1}{2} - i\nu_1; 1|x\right) \tag{A.6}
\end{aligned}$$

For the non planar piece;

$$\begin{aligned}
\Lambda(\nu | \nu_1, \nu_2) &= 2\pi^2 \frac{\Gamma(\frac{1}{2} - i\nu_2) \Gamma(\frac{1}{2} + i\nu + i\nu_1 - i\nu_2)}{\Gamma(\frac{1}{2} + i\nu) \Gamma(\frac{1}{2} + i\nu_1) \Gamma(1 + i\nu - i\nu_2) \Gamma(1 - i\nu - i\nu_2)} \\
&\times {}_3F_2\left(\frac{1}{2} + i\nu_1, \frac{1}{2} - i\nu_1, \frac{1}{2} - i\nu_2 \mid 1 + i\nu - i\nu_2, 1 - i\nu - i\nu_2 \mid 1\right) \\
&\times \frac{\Gamma(\frac{1}{2} - i\nu_1) \Gamma(\frac{1}{2} - i\nu) \Gamma(\frac{1}{2} + i\nu + i\nu_1 + i\nu_2) \Gamma(\frac{1}{2} - i\nu + i\nu_1 + i\nu_2)}{\Gamma(1 - i\nu + i\nu_2) \Gamma(1 + i\nu_1 + i\nu_2)} \\
&\times {}_3F_2\left(\frac{1}{2} + i\nu_1, \frac{1}{2} - i\nu, \frac{1}{2} - i\nu + i\nu_1 + i\nu_2 \mid 1 - i\nu + i\nu_2, 1 + i\nu_1 + i\nu_2 \mid 1\right) \quad (\text{A.7})
\end{aligned}$$

In ref. [1] it was shown that $\Omega(\nu | \nu_1, \nu_2)$ and $\Lambda(\nu | \nu_1, \nu_2)$ are symmetric under cyclic permutations of $\{\nu, \nu_1, \nu_2\}$. That is;

$$\Omega(\nu | \nu_1, \nu_2) = \Omega(\nu_2 | \nu, \nu_1) = \Omega(\nu_1 | \nu_2, \nu)$$

$$\Lambda(\nu | \nu_1, \nu_2) = \Lambda(\nu_2 | \nu, \nu_1) = \Lambda(\nu_1 | \nu_2, \nu) \quad (\text{A.8})$$

with an identical result for the complex conjugates. For specific values of the conformal variables $\{\nu, \nu_1, \nu_2\}$, inserting the appropriate values into Eq. (A.6);

$$\Omega(i\nu | i\nu_1, i\nu_2) = \Omega\left(i\nu \mid \frac{1}{2}, \frac{1}{2}\right) = 2\pi^3 \frac{(1 - i\nu_1 - i\nu_2)}{(1/2 - i\nu_1)^2 (1/2 - i\nu_2)^2} \quad (\text{A.9})$$

$$\Omega^*(i\nu | i\nu_1, i\nu_2) = \Omega\left(i\nu \mid -\frac{1}{2}, -\frac{1}{2}\right) = \frac{4\pi^3}{(1/2 + i\nu)(1/2 - i\nu)} \Re\left(\psi(1) - \psi\left(\frac{1}{2} + i\nu\right)\right) \quad (\text{A.10})$$

$$\Omega(i\nu | i\nu_1, i\nu_2) = \Omega\left(\frac{1}{2} \mid 0, 0\right) = \frac{\pi^5}{1/2 - i\nu} + \frac{2\pi^3}{(1/2 - i\nu)^2} {}_3F_2\left\{\frac{1}{2}, \frac{1}{2}, \frac{1}{2} \mid 1, \frac{3}{2} \mid 1\right\} \quad (\text{A.11})$$

$$\Omega^*(i\nu | i\nu_1, i\nu_2) = \Omega\left(-\frac{1}{2} \mid 0, 0\right) = \frac{2\pi^5}{(1/2 + i\nu)} \quad (\text{A.12})$$

Similarly from Eq. (A.7);

$$\Lambda(i\nu|i\nu_1, i\nu_2) = \Lambda\left(i\nu\left|\frac{1}{2}, \frac{1}{2}\right.\right) = \frac{2\pi^2}{(1/2 - i\nu_1)(1/2 - i\nu_2)} \quad (\text{A.13})$$

$$\Lambda^*(i\nu|i\nu_1, i\nu_2) = \Lambda\left(i\nu\left|-\frac{1}{2}, -\frac{1}{2}\right.\right) = \frac{2\pi^2}{(1/2 + i\nu)(1/2 - i\nu)} \quad (\text{A.14})$$

$$\Lambda(i\nu|i\nu_1, i\nu_2) = \Lambda\left(\frac{1}{2}\left|0, 0\right.\right) = \frac{\pi^2}{(1/2 - i\nu)^2} \quad (\text{A.15})$$

$$\Lambda^*(i\nu|i\nu_1, i\nu_2) = \Lambda\left(-\frac{1}{2}\left|0, 0\right.\right) = \frac{\pi^2}{(1/2 + i\nu)^2} \quad (\text{A.16})$$

Collecting the above results and inserting them into Eq. (A.3), one finds that the planar piece gives a first order pole at $\{\nu, |\nu_1|, |\nu_2|\} = \{0, 1/2, 1/2\}$ and the non planar piece is finite in this region, so that the planar piece is the dominant term for this region. For the region $\{|\nu|, \nu_1, \nu_2\} = \{1/2, 0, 0\}$ one finds the reverse, namely the planar piece is finite whereas the non planar piece offers a first order pole at $\{|\nu|, \nu_1, \nu_2\} = \{1/2, 0, 0\}$, so that the non planar piece is the relevant part of the triple Pomeron vertex for this region;

$$\begin{aligned} \Gamma(i\nu|i\nu_1, i\nu_2) &= \Gamma\left(i\nu\left|\frac{1}{2}, \frac{1}{2}\right.\right) = 32\pi^3\bar{\alpha}_s^2 \frac{(\frac{1}{2} - i\nu)^2 (\frac{1}{2} + i\nu)^2}{(1/2 - i\nu_1)(1/2 - i\nu_2)} \\ &\times \left\{ \frac{1 - i\nu_1 - i\nu_2 - 2/N_c^2}{(1/2 - i\nu_1)(1/2 - i\nu_2)} + \frac{2}{N_c^2}\chi(\nu) \right\} \end{aligned} \quad (\text{A.17})$$

$$\Gamma^*(i\nu|i\nu_1, i\nu_2) = \Gamma\left(i\nu\left|-\frac{1}{2}, -\frac{1}{2}\right.\right) = (4\pi)^3 \bar{\alpha}_s^2 \left(\frac{1}{2} + i\nu\right) \left(\frac{1}{2} - i\nu\right) \left(1 - \frac{1}{N_c^2}\right) \chi(\nu) \quad (\text{A.18})$$

$$\Gamma(i\nu|i\nu_1, i\nu_2) = \Gamma\left(\frac{1}{2}\left|0, 0\right.\right) = \frac{32\pi^3\bar{\alpha}_s^2}{N_c^2} \frac{1}{1/2 - i\nu} \quad (\text{A.19})$$

$$\Gamma^*(i\nu|i\nu_1, i\nu_2) = \Gamma\left(-\frac{1}{2}\left|0, 0\right.\right) = \frac{32\pi^3\bar{\alpha}_s^2}{N_c^2} \frac{1}{1/2 + i\nu} \quad (\text{A.20})$$

The following notation is used for the product of two expressions of the triple Pomeron vertex with specific values, where one is the complex conjugate of the other;

$$\Gamma(i\nu|i\nu_1, i\nu_2) \times \Gamma^*(i\nu|i\nu_1, i\nu_2) \equiv \left| \Gamma(\nu|\nu_1, \nu_2) \right|^2 \quad (\text{A.21})$$

In this notation, combining Eq. (A.17) and Eq. (A.18) yields;

$$\begin{aligned}
\left| \Gamma(\nu|\nu_1, \nu_2) \right|^2 &= \left| \Gamma\left(\nu\left|\frac{1}{2}, \frac{1}{2}\right.\right) \right|^2 = 32 (2\pi)^6 \bar{\alpha}_s^4 \left(1 - \frac{1}{N_c^2}\right) \chi(\nu) \frac{\left(\frac{1}{2} - i\nu\right)^3 \left(\frac{1}{2} + i\nu\right)^3}{(1/2 - i\nu_1)(1/2 - i\nu_2)} \\
&\times \left\{ \frac{1 - i\nu_1 - i\nu_2 - 2/N_c^2}{(1/2 - i\nu_1)(1/2 - i\nu_2)} + \frac{2}{N_c^2} \chi(\nu) \right\}
\end{aligned} \tag{A.22}$$

and collecting the results of Eq. (A.19) and Eq. (A.20);

$$\left| \Gamma(\nu|\nu_1, \nu_2) \right|^2 = \left| \Gamma\left(\frac{1}{2}|0, 0\right) \right|^2 = \left(\frac{32\pi^3 \bar{\alpha}_s^2}{N_c^2} \right)^2 \frac{1}{(1/2 + i\nu)(1/2 - i\nu)} + \text{finite terms} \tag{A.23}$$

B. The fan diagram

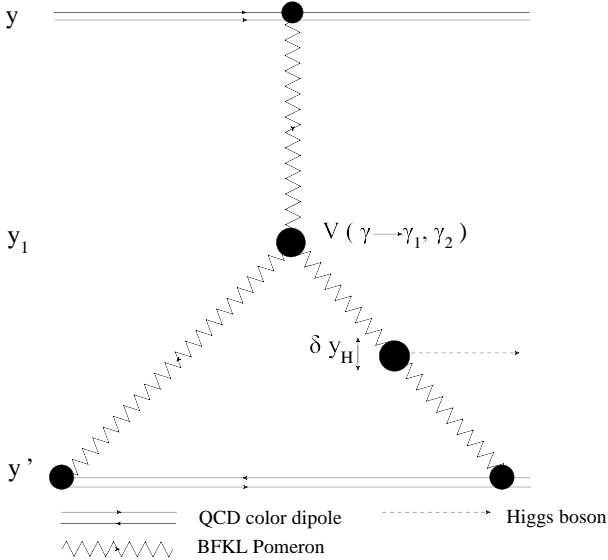


Figure 26: The first fan diagram with $N = 1$ generations of branching.

In this section of the appendix the amplitude of the diagram of Fig. 26 known as the Pomeron “fan” diagram is calculated. The first fan diagram is shown in Fig. 26, where the t-channel Pomeron splits into two daughter Pomerons, and the Higgs boson is produced from one branch of the fan diagram. The scattering is between two QCD dipoles separated by a rapidity gap $\Delta = y - y'$ in rapidity space, and the Pomeron vertex where the splitting occurs is at rapidity y_1 where $y' + \delta y_H \leq y_1 \leq y$. The motivation for this inequality condition is to ensure that the scattering is energetic enough to produce the Higgs boson, and therefore the separation in rapidity space between the vertex at the top of the fan and the target dipole should be at least δy_H . In the representation of complex angular momentum $\omega = 1 + j$ the fan diagram amplitude of Fig. 26 has the expression;

$$\begin{aligned}
F(\omega, \omega_1 | \text{Fig. 26}) &= \frac{1}{S} \left(\frac{\alpha_s}{4} \right)^3 A_H \int \mathcal{D}\gamma \int \mathcal{D}\gamma_1 \int \mathcal{D}\gamma_2 g_\omega(\gamma) g_{\omega_1}(\gamma_1) g_{\omega-\omega_1}(\gamma_2) E_\gamma E_{\gamma_1} E_{\gamma_2} \\
&\times \int d^2 R \int d^2 R_1 \int d^2 R_2 V(R, R_1, R_2 | \gamma \rightarrow \gamma_1, \gamma_2)
\end{aligned} \tag{B.1}$$

where following all the conventions of section 2, the $g_\omega(\gamma)$ are the propagators of the three BFKL Pomeron states in Fig. 26 and the E_γ represent the couplings of the BFKL Pomeron propagators to the

QCD color dipoles. S is the order of the symmetry group of Fig. 26. Including the 2 ways of attaching the Pomeron branch lines at the vertex, and the 2 permutations of the reggeized gluon lines in the triple Pomeron vertex shown in Fig. 10, the total symmetry factor in Eq. (B.1) is $S = 4$. The reason behind the coefficient $(\alpha_s/4)^3$ in Eq. (B.1) follows from similar arguments given in section 2. In Fig. 26 there are three vertices where the BFKL Pomeron couples to the QCD color dipole, namely at the top of the diagram and twice at the lower ends of the two fan branches. Each vertex brings a factor of α_s on account of the 2 couplings of each of the 2 reggeized gluons in the BFKL Pomeron structure (see Fig. 5). Each Pomeron - dipole vertex contains a 4 - fold degeneracy, since both of the 2 reggeized gluons can couple to either of the 2 quark lines in the color dipole, making a total of 4 identical possibilities for each vertex. Thus one arrives at a factor of $\alpha_s/4$ for each of the three vertices in Fig. 26, which ensures that identical diagrams are not counted more than once.

$V(R, R_1, R_2|\gamma \rightarrow \gamma_1, \gamma_2)$ denotes the triple Pomeron vertex for the splitting of the BFKL Pomeron state labeled by the curly brackets (γ is the conformal variable and R is the center of mass coordinate) $\{R, \gamma\}$, into the two BFKL Pomeron states labeled by $\{R_1, \gamma_1\}$ and $\{R_2, \gamma_2\}$ (see Fig. 10). Recall from section 3, that from the condition of conformal invariance comes from the property for the triple Pomeron vertex [1]

$$V(R, R_1, R_2|\gamma \rightarrow \gamma_1, \gamma_2) = R_{01}^{-\Delta_{01}} R_{12}^{-\Delta_{12}} R_{20}^{-\Delta_{20}} R_{01}^{*\tilde{\Delta}_{01}} R_{12}^{*\tilde{\Delta}_{12}} R_{20}^{*\tilde{\Delta}_{20}} \Gamma(\gamma|\gamma_1, \gamma_2) \quad (\text{B.2})$$

where $R_{0i} = R - R_i$ ($i = 1, 2$) and $R_{12} = R_1 - R_2$, and where for example $\Delta_{01} = \gamma + \gamma_1 - \gamma_2$, and $\Delta_{12} = \gamma_1 + \gamma_2 - \gamma$, with an equivalent definition for the $\tilde{\Delta}$ in terms of the $\tilde{\gamma}$. Therefore using this property, Eq. (B.1) can be recast as;

$$F(\omega, \omega_1|\text{Fig. 26}) = \frac{1}{4} \left(\frac{\alpha_s}{4}\right)^3 A_H \int \mathcal{D}\gamma \int \mathcal{D}\gamma_1 \int \mathcal{D}\gamma_2 g_\omega(\gamma) g_{\omega_1}(\gamma_1) g_{\omega-\omega_1}(\gamma_2) E_\gamma E_{\gamma_1} E_{\gamma_2} \times g(\gamma|\gamma_1, \gamma_2) \Gamma(\gamma|\gamma_1, \gamma_2) \quad (\text{B.3})$$

where $g(\gamma|\gamma_1, \gamma_2)$ represents the integral over the center of mass coordinates of the three BFKL states;

$$g(\gamma|\gamma_1, \gamma_2) = \int d^2 R \int d^2 R_1 \int d^2 R_2 (R_{01} R_{01}^*)^{\beta_{01}} (R_{12} R_{12}^*)^{\beta_{12}} (R_{20} R_{20}^*)^{\beta_{20}} \quad (\text{B.4})$$

$$\begin{aligned} \text{where [8]} \quad \beta_{01} &= -\frac{1}{2} - \frac{1}{2} (n - n_1 + n_2) + (i\nu - i\nu_1 + i\nu_2) \\ \beta_{12} &= -\frac{1}{2} + \frac{1}{2} (n + n_1 + n_2) - (i\nu + i\nu_1 + i\nu_2) \\ \beta_{20} &= -\frac{1}{2} + \frac{1}{2} (-n - n_1 + n_2) + (i\nu + i\nu_1 - i\nu_2) \end{aligned} \quad (\text{B.5})$$

Substituting for $g_\omega(\gamma)$ the explicit expression of Eq. (2.12) and switching to rapidity representation (using the above explained inequality $y' + \delta y_H \leq y_1 \leq y$ for the integration limits of the vertex rapidity y_1);

$$\begin{aligned}
F(\Delta, \delta y_H | \text{Fig. 26}) &= \int_{y'+\delta y_H}^y dy_1 \int_{a-i\infty}^{a+i\infty} \frac{d\omega}{2\pi i} e^{\omega\Delta} \int_{a-i\infty}^{a+i\infty} \frac{d\omega_1}{2\pi i} e^{\omega(y_1-y'+\delta y_H)} F_{(1)}(\omega, \omega_1) \\
&= \left(\frac{\alpha_s}{4}\right)^3 A_H \int_{y'+\delta y_H}^y dy_1 \int \mathcal{D}\gamma \lambda(\gamma) e^{\omega(\gamma)\Delta} \\
&\quad \times \frac{1}{4} \int \mathcal{D}\gamma_1 \int \mathcal{D}\gamma_2 \lambda(\gamma_1) \lambda(\gamma_2) \exp\{(\omega(\gamma_1) + \omega(\gamma_2) - \omega(\gamma))(y_1 - y') - \omega(\gamma_1)\delta y_H\} \\
&\quad \times E_\gamma E_{\gamma_1} E_{\gamma_2} g(\gamma|\gamma_1, \gamma_2) \Gamma(\gamma|\gamma_1, \gamma_2)
\end{aligned} \tag{B.6}$$

where $\Delta = y - y'$ is the rapidity gap between the scattering dipoles in Fig. 26. The leading contribution stems from the region where all conformal spins $\{n, n_1, n_2\} = 0$ since the BFKL eigenfunction $\omega(n, \nu)$ decreases sharply as n increases, and is positive only for $n = 0$ at high energies. Therefore ignoring all solutions where $\{n, n_1, n_2\} \neq 0$, and using the explicit expression of Eq. (2.10) for the integration measure Eq. (B.6) reduces to;

$$\begin{aligned}
F(\Delta, \delta y_H | \text{Fig. 26}) &= \left(\frac{\alpha_s}{4}\right)^3 A_H \int_{y'+\delta y_H}^y dy_1 \int_{-\infty}^{\infty} d\nu h(\nu) \lambda(\nu) e^{\omega(\nu)\Delta} \\
&\quad \times \frac{1}{4} \int_{-\infty}^{\infty} d\nu_1 h(\nu_1) \lambda(\nu_1) \int d\nu_2 h(\nu_2) \lambda(\nu_2) e^{(\omega(\nu_1) + \omega(\nu_2) - \omega(\nu))(y_1 - y') - \omega(\nu_1)\delta y_H} \\
&\quad \times E_\nu E_{\nu_1} E_{\nu_2} g(\nu|\nu_1, \nu_2) \Gamma(\nu|\nu_1, \nu_2) \\
&= \frac{\bar{\alpha}_s^3 A_H}{2^8 \pi N_c^3} \int_{-\infty}^{\infty} d\nu \frac{\nu^2}{(1/2 + i\nu)^2 (1/2 - i\nu)^2} e^{\omega(\nu)\Delta} E_\nu f(\nu|\Delta, \delta y_H)
\end{aligned} \tag{B.7}$$

$$\begin{aligned}
\text{where } f(\nu|\Delta, \delta y_H) &= \frac{1}{2^7 \pi^8} \int_{-\infty}^{\infty} \frac{d\nu_1 \nu_1^2}{(1/2 + i\nu_1)^2 (1/2 + i\nu_1)^2} \int_{-\infty}^{\infty} \frac{d\nu_2 \nu_2^2}{(1/2 + i\nu_2)^2 (1/2 - i\nu_2)^2} \\
&\quad \times \int_{y'+\delta y_H}^y dy_1 \exp\{(\omega(\nu_1) + \omega(\nu_2) - \omega(\nu))(y_1 - y') - \omega(\nu_1)\delta y_H\} \\
&\quad \times E_{\nu_1} E_{\nu_2} g(\nu|\nu_1, \nu_2) \Gamma(\nu|\nu_1, \nu_2)
\end{aligned} \tag{B.8}$$

Eq. (B.8) represents the contribution of the fan part of the diagram of Fig. 26. The leading contribution to Eq. (B.8) stems from the region $\{|\nu|, \nu_1, \nu_2\} = \{1/2, 0, 0\}$ which was discussed in the previous sections for solving the Pomeron loop integrals. For this region, $g(\nu|0, 0)$ can be calculated from Eq. (B.4), by

choosing the frame of reference where one of the center of mass coordinates $R = 0$. With this choice of frame after evaluating the remaining integrations over R_1 and R_2 it turns out that;

$$g(\nu|0,0) = \frac{16\pi^3}{1/2 - i\nu} \quad (\text{B.9})$$

After substituting Eq. (B.9) and the triple Pomeron vertex of Eq. (A.19) into Eq. (B.8), the integrals over ν_1 and ν_2 can be solved using the method of steepest descents. Plugging the result back into Eq. (B.7) yields the expression;

$$\begin{aligned} F(\Delta, \delta y_H | \text{Fig. 26}) &= \frac{2\bar{\alpha}_s^5 A_H}{N_c^5 \pi^2 [\omega''(0)]^3} \oint_C d\nu \frac{\nu^2}{(1/2 + i\nu)^2 (1/2 - i\nu)^4} E_\nu \\ &\times \int_{y'+\delta y_H}^y dy_1 e^{\omega(\nu)(y-y_1)} \frac{e^{2\omega(0)(y_1-y'-\delta y_H/2)}}{(y_1 - y')^{3/2} (y_1 - y' - \delta y_H)^{3/2}} \end{aligned} \quad (\text{B.10})$$

where C is the contour shown in Fig. 13 which encloses the pole at $i\nu = 1/2$, and a factor of 2 has been included which takes into account the identical contribution from the contour C' , which encloses the pole at $i\nu = -1/2$. One can solve the ν integral using the same technique shown in Eq. (3.24), which generates the derivative of the Dirac delta function $\delta^{(2)}(y - y_1) / \bar{\alpha}_s^2$, and this is absorbed by the integration over the rapidity variable y_1 to finally yield;

$$\begin{aligned} F(\Delta, \delta y_H | \text{Fig. 26}) &= \frac{2\bar{\alpha}_s^2 A_H}{N_c^5 \pi [\omega''(0)]^3} \frac{d^2}{d\Delta^2} \left(\frac{e^{2\omega(0)(\Delta - \delta y_H/2)}}{\Delta^{3/2} (\Delta - \delta y_H)^{3/2}} \right) \\ &= 2.93 \times 10^{-11} \text{ GeV}^{-2} \quad (\alpha_s = 0.12) \\ &= 3.95 \times 10^{-8} \text{ GeV}^{-2} \quad (\alpha_s = 0.2) \end{aligned} \quad (\text{B.11})$$

References

- [1] G. P. Korchemsky, *Nucl. Phys. B* **550** (1999) 397 [arXiv:hep-ph/9711277].
- [2] A. Bialas, H. Navelet, R. Peschanski, [arXiv:hep-ph/9711442].
- [3] J. S. Miller, *Eur. Phys. J. C* **56** (2008) 39 - 55 [arXiv:hep-ph/0610427].
- [4] E. Gotsman, E. Levin, U. Maor and J. S. Miller, *Eur. Phys. J. C* **57** (2008) 689 [arXiv:0805.2799 [hep-ph]].
- [5] A. H. Mueller, *Nucl. Phys. B* **437** (1995) 107 [arXiv:hep-ph/9408245].
- [6] Y. Kovchegov, *Phys. Rev. D* **72** (2005) 094009 arXiv:hep-ph/0508276
- [7] E. Levin, J. Miller and A. Prygarin, *Nucl. Phys. A* **806**, 245 (2008) [arXiv:0706.2944 [hep-ph]].

- [8] M. Braun, [arXiv:0901.3660 [hep-ph]].
- [9] H. Navelet and R. B. Peschanski, *Nucl. Phys.* **B 634** (2002) 291 [arXiv:hep-ph/0201285].
- [10] H. Navelet and R. B. Peschanski, *Phys. Rev. Lett.* **82** (1999) 1370 [arXiv:hep-ph/9809474].
- [11] A. Bialas, H. Navelet and R. B. Peschanski, *Phys. Lett.* **B 427** (1998) 147 [arXiv:hep-ph/9711236].
- [12] M. Kozlov and E. Levin, *Nucl. Phys.* **A 739**, 291 (2004) [arXiv:hep-ph/0401118].
- [13] J. Ellis et al., *Nucl. Phys.* **B106** (1976) 326-331
- [14] T. G. Rizzo, *Phys. Rev.* **D22** (1980) 178, Addendum-ibid *Phys. Rev.* **D22** (1980) 1824-1825
- [15] S. Dawson, *Nucl. Phys.* **B359** (1991) 283-300
- [16] S. Bentvelsen, E. Laenen, P. Motylinski, NIKHEF 2005 - 007
- [17] J. Ellis et al., *Nucl. Phys.* **B106** 326- 331 (1976)
- [18] J. S. Miller, arXiv:0704.1985 [hep-ph].
- [19] S. Bravo, I. Gallart, “*Measurements of the strong coupling constant and the QCD colour factors using four-jet observables from hadronic Z decays in ALEPH. ((B))*,” CERN-THESIS-2002-034;
A. Heister *et al.* [ALEPH Collaboration], “*Measurements of the strong coupling constant and the QCD colour factors using four-jet observables from hadronic Z decays*,” *Eur. Phys. J.* **C 27** (2003) 1-17.
- [20] J. Foreshaw, D. Ross, Quantum Chromodynamics and the Pomeron. Cambridge University Press, p 93

